④

The Magnetospheric Response to 8-Minute Period Strong-Amplitude Upstream Pressure Variations

D. G. SIBECK, A. T. Y. LUI, R. W. McENTIRE, T. A. POTEMRA, and K. TAKAHASHI
John Hopkins University
Laurel, MD 21218

W. BAUMJOHANN
Institut fuer Extraterrestrische Physik
Federal Republic of Germany

R. C. ELPHIC
University of California
Los Angeles, CA 90024

D. H. FAIRFIELD
Nasa Goddard Space Flight Center
Greenbelt, MD 20771

J. F. FENNELL and W. B. GAIL
The Aerospace Corporation
El Segundo, CA 90245

L. J. LANZEROTTI and C. G. MACLENNAN
AT&T Bell Laboratories
Murray Hill, NJ 07974

R. E. LOPEZ
Applied Research Corporation
Landover, MD 20784

H. LUEHR
Technische Universitaet Braunschweig
Federal Republic of Germany

and

T. J. ROSENBERG
University of Maryland
College Park, MD 20740

6 August 1990

Prepared for

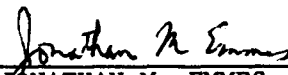AD-A228 038

DTIC
ELECTE
NOV 02 1990
S B D

This report was submitted by The Aerospace Corporation, El Segundo, CA 90245, under Contract No. F04701-88-C-0089 with the Space Systems Division, P.O. Box 92960, Los Angeles, CA 90009-2960. It was reviewed and approved for The Aerospace Corporation by A. B. Christensen, Director, Space Sciences Laboratory. Lt T. Fisher was the project officer for the Mission-Oriented Investigation and Experimentation (MOIE) Program.

This report has been reviewed by the Public Affairs Office (PAS) and is releasable to the National Technical Information Service (NTIS). At NTIS, it will be available to the general public, including foreign nationals.

This technical report has been reviewed and is approved for publication. Publication of this report does not constitute Air Force approval of the report's findings or conclusions. It is published only for the exchange and stimulation of ideas.

TYRON FISHER, LT, USAF
MOIE Project Officer
SSD/CLPO

JONATHAN M. EMMES, MAJ, USAF
MOIE Program Manager
AFSTC/WCO OL-AB

REPORT DOCUMENTATION PAGE

1a. REPORT SECURITY CLASSIFICATION	1b. RESTRICTIVE MARKINGS
Unclassified	

2a. SECURITY CLASSIFICATION AUTHORITY	3. DISTRIBUTION/AVAILABILITY OF REPORT
2b. DECLASSIFICATION/DOWNGRADING SCHEDULE	Approved for public release; distribution unlimited.

4. PERFORMING ORGANIZATION REPORT NUMBER(S)	5. MONITORING ORGANIZATION REPORT NUMBER(S)
TR-0089(4940-05)-1	SSD-TR-89-30

6a. NAME OF PERFORMING ORGANIZATION	6b. OFFICE SYMBOL (If applicable)	7a. NAME OF MONITORING ORGANIZATION
The Aerospace Corporation Laboratory Operations		Space Systems Division

6c. ADDRESS (City, State, and ZIP Code)	7b. ADDRESS (City, State, and ZIP Code)
El Segundo, CA 90245-4691	Los Angeles Air Force Base Los Angeles, CA 90009-2960

8a. NAME OF FUNDING/SPONSORING ORGANIZATION	8b. OFFICE SYMBOL (If applicable)	9. PROCUREMENT INSTRUMENT IDENTIFICATION NUMBER
		F04701-88-C-0089

8c. ADDRESS (City, State, and ZIP Code)	10. SOURCE OF FUNDING NUMBERS			
	PROGRAM ELEMENT NO.	PROJECT NO.	TASK NO.	WORK UNIT ACCESSION NO.

11. TITLE (Include Security Classification)
The Magnetosphere Response to 8-Minute Period Strong-Amplitude Upstream Pressure Variations

12. PERSONAL AUTHOR(S) Sibeck, D. G.; Lui, A. T. Y.; McEntire, R. W.; Potemra, T. A.; and Takahashi, K. (John Hopkins University) Baumjohann, W. (Institut fuer Extraterrestrische

13a. TYPE OF REPORT	13b. TIME COVERED	14. DATE OF REPORT (Year, Month, Day)	15. PAGE COUNT
	FROM _____ TO _____	1990 August 6	61

16. SUPPLEMENTARY NOTATION

17. COSATI CODES			18. SUBJECT TERMS (Continue on reverse if necessary and identify by block number)
FIELD	GROUP	SUB-GROUP	Solar wind

19. ABSTRACT (Continue on reverse if necessary and identify by block number)

This report documents a series of brief, strong ($\Delta p/p = 1$), dynamic pressure oscillations that occurred in the region upstream of the Earth's bow shock during a period of radial interplanetary magnetic field (IMF). The analyzed set of oscillations, which may be either intrinsic solar wind or bow shock-related phenomena, recur approximately every 8 to 10 minutes, and their magnetic field signatures occur nearly simultaneously over great distances transverse to the Earth-sun line. The pressure oscillations appear to drive tailward-moving magnetopause surface wavelets. In turn, the surface wavelets can be identified as hydromagnetic waves with strong compressional components in the outer magnetosphere and as quasi-periodic variations in electron precipitation and high-latitude ground pulsations. We use observations by spacecraft in the outer dayside magnetosphere to predict geosynchronous and subsolar magnetic field strengths, the location of the subsolar magnetopause, the solar wind dynamic pressure, and variations in the energetic magnetospheric ion flux.

20. DISTRIBUTION/AVAILABILITY OF ABSTRACT	21. ABSTRACT SECURITY CLASSIFICATION
☒ UNCLASSIFIED/UNLIMITED ☐ SAME AS RPT. ☐ DTIC USERS	Unclassified

22a. NAME OF RESPONSIBLE INDIVIDUAL	22b. TELEPHONE (Include Area Code)	22c. OFFICE SYMBOL

DD FORM 1473, 84 MAR 83 APR edition may be used until exhausted. All other editions are obsolete SECURITY CLASSIFICATION OF THIS PAGE

12. PERSONAL AUTHORS (Continued)

Physik) Elphic, R. C. (UCLA), Fairfield, D.H. (NASA GSFC), Fennell, J. F. and Gail, W. B. (The Aerospace Corporation), Lanzerotti, L. J. and Maclennan, C. G. (AT&T Bell Laboratories), Lopez, R. E. (Applied Research Corporation), Luehr, H. (Technische Universitaet Braunschweig), and Rosenberg, T. J. (University of Maryland)

PREFACE

Accession For

NTIS GRA&I	☑
DTIC TAB	☐
Unannounced	☐
Justification	

By

Distribution/

Availability Codes

Dist	Avail and/or Special
A-1	

1

CONTENTS

FIGURES (Continued)

I. INTRODUCTION

The characteristics of geomagnetic pulsations potentially provide a great deal of information about the near-Earth environment. However, without simultaneous multipoint measurements, it can be difficult to distinguish the origin of the pulsations and decode the information that they convey. Notable causes of geomagnetic pulsations include internal magnetospheric instabilities, magnetopause instabilities, and upstream waves (T ~20-100 s) generated at the bow shock. We will present observations of quasi-periodic (τ = 500 s) compressional magnetospheric fluctuations and, on the basis of simultaneous multipoint measurements, conclude that their characteristics are inconsistent with the known properties of any of these sources. Rather, the observations suggest the presence of rarely discussed, strongly compressional intrinsic solar wind or bow shock-generated fluctuations with periods of 200 to 600 s.

This study begins with an extensive review of possible causes of magnetospheric pulsations with frequencies of 30 to 600 s. The purpose of this review is threefold: (1) to establish the characteristics of the various competing mechanisms for magnetospheric pulsations, (2) to place recent conflicting statements about the origin of magnetospheric pulsations with periods of 200 to 600 s in context, and (3) to provide a basis for interpreting the new observations presented in this report. The review demonstrates the importance of multipoint measurements in distinguishing the origin of pulsations. Following this review, we will present and then discuss simultaneous observations of oscillations with ~500-s periods on the ground, in the outer magnetosphere, and upstream of the bow shock. We will examine the extent to which simple magnetospheric models can be used to predict upstream solar wind dynamic pressure variations from magnetospheric observations, the magnetic signal seen at one magnetospheric satellite from another, and the response of energetic magnetospheric ions to compressional oscillations. In summary, we will demonstrate the

7

presence of short-period upstream dynamic pressure variations and their importance in driving magnetospheric oscillations with periods of about 200 to 600 s.

II. REVIEW

In this section, we review what is known about the response of the dayside magnetospheric magnetic field to various phenomena, including step-function increases in solar wind dynamic pressure, shorter period variations in solar wind dynamic pressure, plasma oscillations at the quasi-parallel bow shock, and magnetopause and magnetospheric instabilities. The review shows that all these phenomena contribute to magnetospheric pulsations with periods of 200 to 600 s. For a different perspective on the sources of these pulsations; see Yumoto.[1]

A. STEP-FUNCTION VARIATIONS IN SOLAR WIND DYNAMIC PRESSURE

Solar wind shocks occur less frequently than one per day and can be considered large-scale and large-amplitude step-functionlike changes in the solar wind pressure. Kaufmann and Konradi[2] illustrated the qualitative effect of a step-function increase in the solar wind pressure upon the ecliptic plane cross section of the magnetosphere. They argued that an abrupt decrease in the magnetopause position would propagate tailward with the shock, leaving behind higher magnetic field strengths in a compressed magnetosphere. Gosling et al.[3,4] and Ogilvie et al.[5] demonstrated direct correlation of dynamic pressure increases at solar wind shocks and tangential discontinuities with sudden impulse (SI) and sudden storm commencement (SSC) increases in the Earth's surface magnetic field. Siscoe,[6] Siscoe et al.,[7] and Smith et al.[8] estimated sudden solar wind pressure changes from measured variations in ground magnetograms. Baumjohann et al.[9] and Wilken et al.[10] have recently used multisatellite observations to study the effects of a passing solar wind shock on the magnetospheric magnetic field, plasma, and energetic particle population.

The sharp changes in solar wind dynamic pressure which produce SIs and SSCs often excite resonant hydromagnetic waves with longer periods in the magnetospheric interior and on the ground [Voelker,[11] Saito and Matsushita,[12] Kaufmann and Walker,[13] Fukunishi,[14] Baumjohann et al.,[15] and Friis-Christensen et al.[16]].

B.   PERIODIC SOLAR WIND VARIATIONS

The solar wind also exhibits variability on much shorter time scales. Burlaga[17,18] reported successive IMF variations in strength and direction that recurred as often as every 200 to 600 s and attributed them to waves, discontinuities, and directional discontinuities. Directional discontinuities can recur as often as several hours[1] [Burlaga,[18] Solodyna, et al.[19], are coherent over large distances transverse to the Earth-sun line, and remain identifiable as they advect antisunward [Ness,[20] Burlaga and Ness[21]]. Burlaga[17] and Siscoe et al.[22] have shown that the magnetic field strength can change by a factor of 2 or more across discontinuities.

It is not clear how such rapid variations in the solar wind magnetic field strength might affect the magnetosphere. However, it is very likely that many of these solar wind magnetic field variations are associated with corresponding solar wind plasma variations. Unfortunately, the properties and occurrence rates of solar wind plasma variations in the ~200 to 600-s period range are poorly known. Burlaga[17] has demonstrated that, in some cases, the solar wind plasma density varies to preserve the sum of the static and magnetic pressures. Were this finding general, one might expect solar wind densities to vary up to a factor of 4 when tangential discontinuities pass. However, Solodyna et al.[19] found few or no cases in which there was more than a 35% change in the density. Burlaga[17] presented no evidence that the solar wind velocity varies so as to preserve the dynamic pressure across discontinuities. Thus, we conclude that the dynamic pressure varies across solar wind tangential discontinuities, but only on rare occasions by a factor of 4.

Now consider the magnetospheric response to these solar wind dynamic pressure variations. As a working hypothesis, we adopt the schematic model shown in Fig. 1 as framework for interpreting the observations that follow. A band of increased solar wind pressure (shaded) passes tailward, compressing that portion of the magnetopause with which it is in contact and increasing the magnetospheric magnetic field. However, the pressure increase is so brief that the dayside magnetosphere never reaches equilibrium before
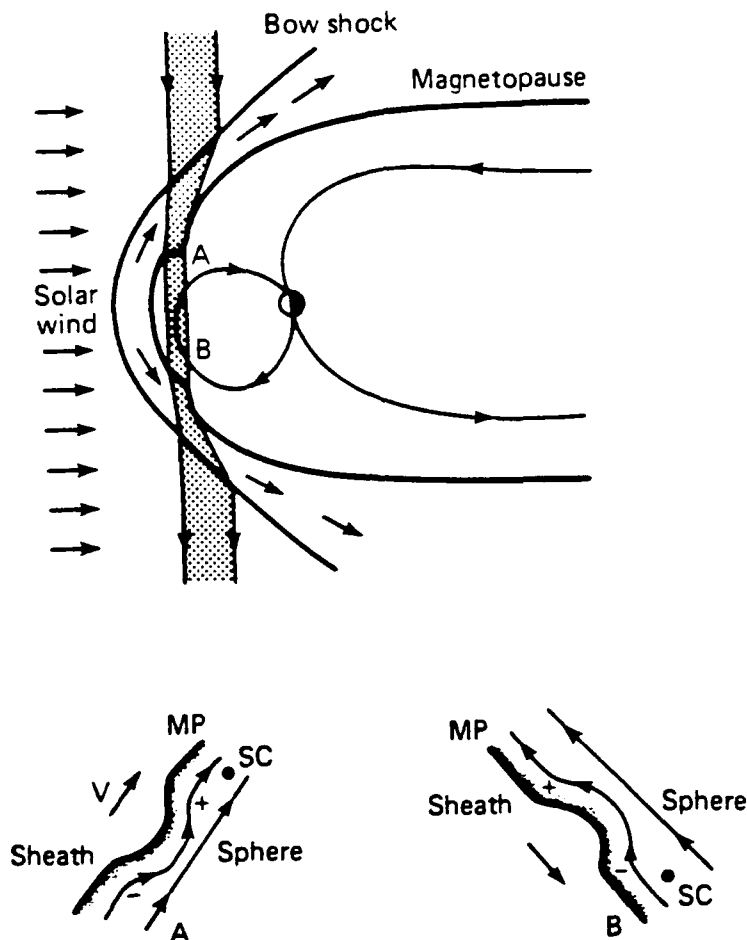
Fig. 1. A Region of Enhanced Solar Wind Dynamic Pressure Passes
         the Earth and its Magnetosphere. The dimensions of the
         region are less in the magnetosheath than in the solar
         wind since the magnetosheath flow is compressed. The
         region of enhanced pressure distorts the magnetospause,
         pushing it inward. The passage of the high-pressure
         region produces a characteristic magnetic field signature
         in the magnetospheric magnetic field: an inward, outward
         bipolar oscillation of the magnetic field component normal
         to the nominal magnetopause south of the equator, and an
         outward, inward bipolar signature north of the equator.
         Magnetic field strengths reach a maximum at the observing
         spacecraft just as the trough of the compression passes,
         unless the spacecraft crosses the magnetopause and enters
         the magnetosheath, a region of low magnetic field strengths.

11

the external pressure returns to its previous value. The increased press-
ure indents the magnetopause (points A and B in Fig. 1), and the ripples
travel tailward with the magnetosheath flow. The indentation amplitude
must increase for larger solar wind pressure increases.

If the only effect of the pressure change is an indentation, then
there will also be a characteristic magnetic field signature. A spacecraft
(SC) inside the dayside magnetopause and north of the point on the magneto-
pause at which the band of increased pressure first made contact (i.e., at
point A) will first observe an outward (plus) magnetic field component
normal to the nominal magnetopause, an increase in the magnetic field
strength as the trough of the indentation passes, and an inward (minus)
magnetic field component normal to the nominal magnetopause position. A
spacecraft inside the magnetopause and south of the point of initial
contact (i.e., at point B) will observe the reverse signature; the inward
(minus) normal component precedes the outward (plus) component. We can
therefore expect (plus, minus) B_n magnetospheric signatures north of the
(near-equatorial) point of first contact and (minus, plus) B_n signatures
south of that point. Finally, if the observing spacecraft is very near the
magnetopause, it may cross that boundary or enter the plasma boundary layer
(shown shaded in the lower two panels) just inside the magnetopause when
the trough passes.

As indirect evidence for such a model, Nishida and Cahill[23] demon-
strated that at least some long-period (~600 s) magnetospheric variations
observed in the outer magnetosphere were also observed in low-latitude
magnetograms. Further, they showed that some increases in the total field
strength at both locations were associated with magnetospheric compressions
and some decreases with expansions. Consequently, they deduced that solar
wind pressure variations drove these magnetospheric magnetic field varia-
tions. Barcus and Rosenberg[24] and Oguti et al.[25] have suggested solar wind
pressure variations as a source for low-altitude pulsations in riometer,
energetic electron flux, and ground magnetic field observations with
periods of ~200 s. Song et al.[26] find that variations in solar wind

dynamic pressure suffice to explain the observed amplitude of magnetopause motion. None of these authors presented simultaneous high time resolution solar wind and magnetosphere observations to verify their theses.

A study by Potemra et al.[27] remedied this situation. They reported a case study with simultaneous IMP-8 solar wind measurements, AMPTE CCE and Viking magnetospheric measurements, and EISCAT Cross ground-based magnetometer observations. This study determined that an isolated ~600-s variation in solar wind density during a period of nearly radial IMF could be directly associated with magnetic field variations with a similar wave form inside the magnetosphere and on the ground.

C. BOW SHOCK PHENOMENA

Wave-particle interactions in the region upstream of the Earth's bow shock are a local source of large-amplitude ($\Delta n/n = 1$), compressional, magnetic field, and plasma oscillations [Paschmann et al.[28]], with typical periods of 20 to 60 s [Fairfield[29]]. These upstream fluctuations are not coherent in amplitude or phase even at nearby satellites [Russell et al.[30]]. Spangler et al.[31] reported two instances in which the upstream density variations were organized into wave packets with periods of ~240 to 300 s.

Simultaneous in situ observations demonstrate that waves generated at the bow shock can excite resonant magnetospheric oscillations with periods of 10 to 100 s [Plyasova-Bakounina et al.[32]]. The frequency of the magnetospheric oscillations and the location of observed waves depend on the upstream wave frequency and plasma conditions of the magnetospheric magnetic field lines [Takahashi et al.[33]]. Miletits et al.[34] have noted that Pc3 ground pulsations can be organized into packets with ~600-s periods. The location and means by which such upstream and magnetospheric waves penetrate the magnetopause and propagate to low latitudes remain unclear, although the cusp and dayside magnetopause have been suggested as possible regions of entry [e.g., Lanzerotti et al.,[35] Yumoto et al.[36]].

13

To our knowledge, there has been no effort to correlate upstream waves or wave packets with periods greater than 100 s with magnetospheric oscillations. If upstream waves and wave packets with these periods were found to be coherent over large distances, the magnetosphere might react to them in the same manner as that outlined above for intrinsic solar wind dynamic pressure variations.

D. MAGNETOPAUSE BOUNDARY PHENOMENA

Here we consider the effects on the magnetospheric magnetic field of two types of magnetopause boundary layer phenomena: Kelvin-Helmholtz waves and flux transfer events (FTEs).

The Kelvin-Helmholtz instability has long been suggested as the cause of some geomagnetic pulsations [Dungey,[37] Atkinson and Watanabe[38]]. Theoretical studies [e.g., Southwood,[39,40] Pu and Kivelson[41]] predict that the instability generates a series of tailward-moving magnetopause boundary waves when the solar wind velocity exceeds some threshold. The wave growth rate increases when magnetosheath and magnetospheric magnetic fields lie transverse to the flow, for lower Alfven velocities, and for sharper velocity shear at the magnetopause. The instability is therefore most likely on the magnetotail flanks (weak transverse magnetosheath magnetic field), for a weak southward IMF (weak transverse magnetosheath magnetic field), and high solar wind densities and velocities. The instability is less-favored when the IMF turns northward because the magnetopause boundary layer thickness increases northward [Mitchell et al.[42]], thereby reducing the shear. Reasonable estimates of Kelvin-Helmholtz boundary wave amplitudes and periods at the magnetopause are ~1 R_E and ~20 to 300 s or longer, respectively [Pu and Kivelson[41]]. The waves should compress and expand the magnetosphere as they move tailward, thereby producing (plus, minus) B_n signatures north of the equator and (minus, plus) B_n signatures south of the equator, as in Fig. 1.

Kivelson et al.[43] have suggested Kelvin-Helmholtz waves at the magnetopause as a cause of global magnetospheric compressions with 500-s

periods. Recent ground magnetometer observations reported by Wolfe et al.[44,45] and geosynchronous electric field observations reported by Junginger and Baumjohann,[46] provide indirect evidence for the Kelvin-Helmholtz instability. These authors report statistical studies indicating that the solar wind velocity, more than any other parameter, controls the occurrence of magnetospheric wave power in the band from 150 to 600 s. McHenry et al.[47] report case and statistical studies of ground pulsations with periods of 1200 s observed in the Greenland magnetometer chain. These pulsations move antisunward, and their amplitude increases with increasing solar wind velocity, consistent with the Kelvin-Helmholtz instability.

Flux transfer events (FTEs) at the dayside magnetopause appear to occur for interplanetary magnetic field orientations that are not strongly northward [Southwood et al.[48] and references therein]. FTEs occur every ~420 to 480 s, have scale sizes of 1 to 2 R_E [Rijnbeek et al.[49]], have characteristic (plus, minus) B_n signatures [Russell and Elphic[50]], move tailward with the magnetosheath flow, and may be associated with Kelvin-Helmholtz driven magnetopause boundary waves [Glassmeier et al.,[51] Lanzerotti and Maclennan[52]]. Magnetospheric FTEs further resemble Kelvin-Helmholtz and upstream pressure variation-driven boundary motion in that the FTE B_n signature is (plus, minus) north of the equatorial merging line and (minus, plus) south of that line [Rijnbeek et al.[49]]. The magnetic field in FTEs often rotates away from both the magnetosheath and magnetosphere orientations, in a manner consistent with twisting. Although this signature may distinguish FTEs from boundary waves {Russell and Elphic[50]}, it can also be a natural feature of field line draping over bumps in the magnetopause [Farrugia et al.[53,54]]. Some FTEs are associated with high-speed flows that may distinguish them from boundary waves [Paschmann et al.[55]]. FTEs may produce ULF hydromagnetic waves with periods of 10 to 100 s in the dayside magnetopause cusp region [Lee et al.[56]] that may propagate to the ground and be observed as pulsations [Goertz et al.,[57] Lanzerotti et al.[58,59]]. Gillis et al.[60] suggested that FTEs generate

waves with periods of 60 to 120 s that penetrate deep into the magneto-sphere, but this had been recently challenged, primarily upon methodological grounds, by Lanzerotti.[66] (Gillis et al.[62] responded with a modified position.)

E.   INTERNAL MAGNETOSPHERIC PHENOMENA

Instabilities in the ring current, ion drift modes in particular, are another mechanism for generating MHD waves with periods of 200 to 600 s. The energy for the instabilities can come from density gradients and/or pressure anisotropies [Hasegawa[63] and Southwood[64]] that are likely during substorm particle injections. Since solar wind conditions control substorm activity, even these internally-excited MHD waves can be considered as ultimately controlled by the solar wind. However, substorm onset lags changes in solar wind conditions and a further lag is introduced during the time required for the unstable plasma from its injection site near midnight to the satellite location. Thus, it is usually easy to distinguish directly driven pulsations and those generated internally as a consequence of substorms.

III. OBSERVATIONS

After discussing the data sets to be presented, we consider the observations, beginning with those in the solar wind, those in the outer magnetosphere, and concluding with those at the ground.

A. DATA

Figure 2 depicts the orbits of six near-equatorial spacecraft projected into the GSE equatorial plane during the period from 1500 to 2000 UT on 10 September 1984. The IMP-8, IRM, and ISEE-2 satellites were upstream of the Earth's bow shock, and the CCE, SCATHA, and GOES-6 satellites were inside the magnetosphere. Ground-based observations are available from the south pole station, which moved through local magnetic noon (MLT ~ UT-3.5)

SEPTEMBER 10, 1984
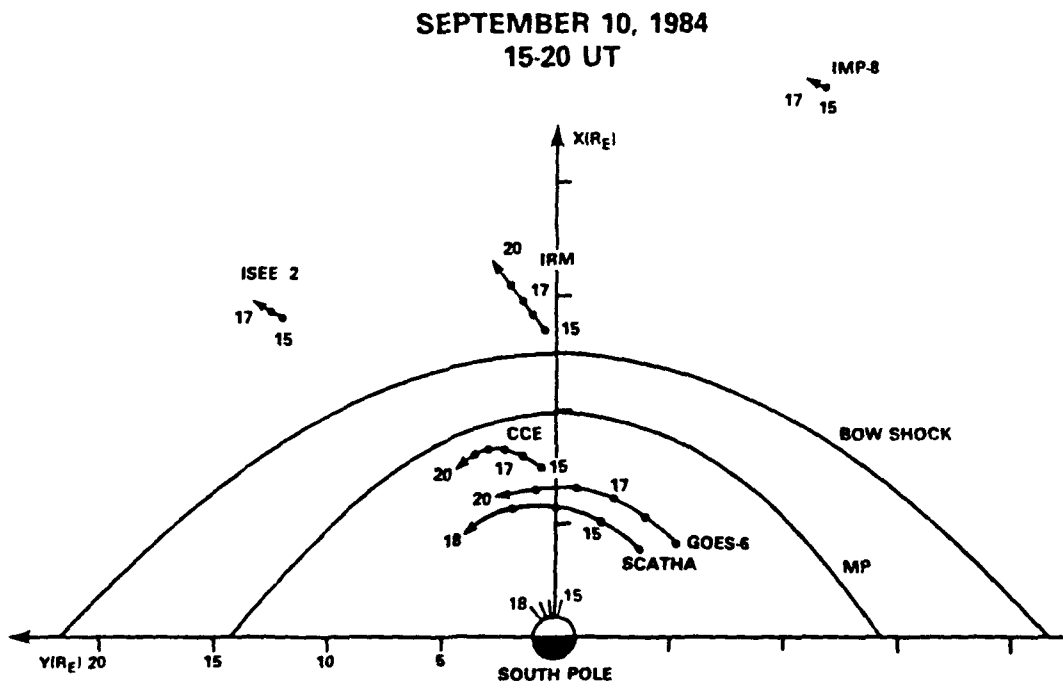**15-20 UT**

Fig. 2. Trajectories of IMP-8, IRM, ISEE-2, GOES-6, CCE, and
         SCATHA During the Period of Interest on 10 September 1984.
         Ticks show the local time motion of south pole station.

17

during this interval. The data sets, 60-s averages except where noted, are described in the following sequence: solar wind, outer magnetosphere, inner magnetosphere, and south pole.

We first present IRM solar wind plasma [Paschmann et al.[65]] and magnetic field [Luehr et al.[66]] measurements. Although IRM plasma measurements are available as often as every 4.35 s, we use 15- to 60-s averages, sufficient to study solar wind plasma microstructures. For IRM electron densities, we use n_e^*, which includes an estimate of the particle density below 15 eV. Then we consider ISEE-2 magnetic field observations [Russell[67]] and IMP-8 magnetic field and plasma measurements [King[68]]. We present CCE magnetospheric magnetic field [Potemra et al.[69]] and energetic ion [McEntire et al.[70]] observations, geosynchronous GOES-6 magnetic field observations [Grubb[71]], and near-geosynchronous SCATHA magnetic field data [Fennell[72]], Finally, we discuss measurements of cosmic radio noise absorption, ELF/VLF emissions, and magnetic field variations obtained at the south pole station [Gail,[73] Lanzerotti, et al.[74]]. The absorption was measured with 20.5, 30, and 51.4 MHz riometer receivers that view a zenith-centered, circular (~100-km diameter) region of the ionosphere at ~90-km height. ELF/VLF emissions were recorded in five frequency bands (0.5-1, 1-2, 2-4, 11-13, and 31-38 kHz) using a receiving system with sensitivity of 6 µV/m and a magnetic loop antenna. Surface variations of the magnetic field were recorded by a three-axis fluxgate magnetometer in a coordinate frame with components in the north-south (H, positive north), east-west (D, positive east), and vertical (Z, positive upward) directions. All data were sampled at the rate of 1 Hz.

B. SOLAR WIND OBSERVATIONS

Figure 3 presents 5 hr of IRM solar wind observations from 1500 to 2000 UT on 10 September 1984. At this time, as Fig. 2 shows, the space-craft was near local noon and had just crossed the bow shock out~ound. From top to bottom, the panels of Fig. 3 show the electron density, the proton velocity, the dynamic pressure ($= n_e M v_p^2$), the electron thermal pressure ($= n_e k T_e$), and the magnetic pressure. The mean solar wind density
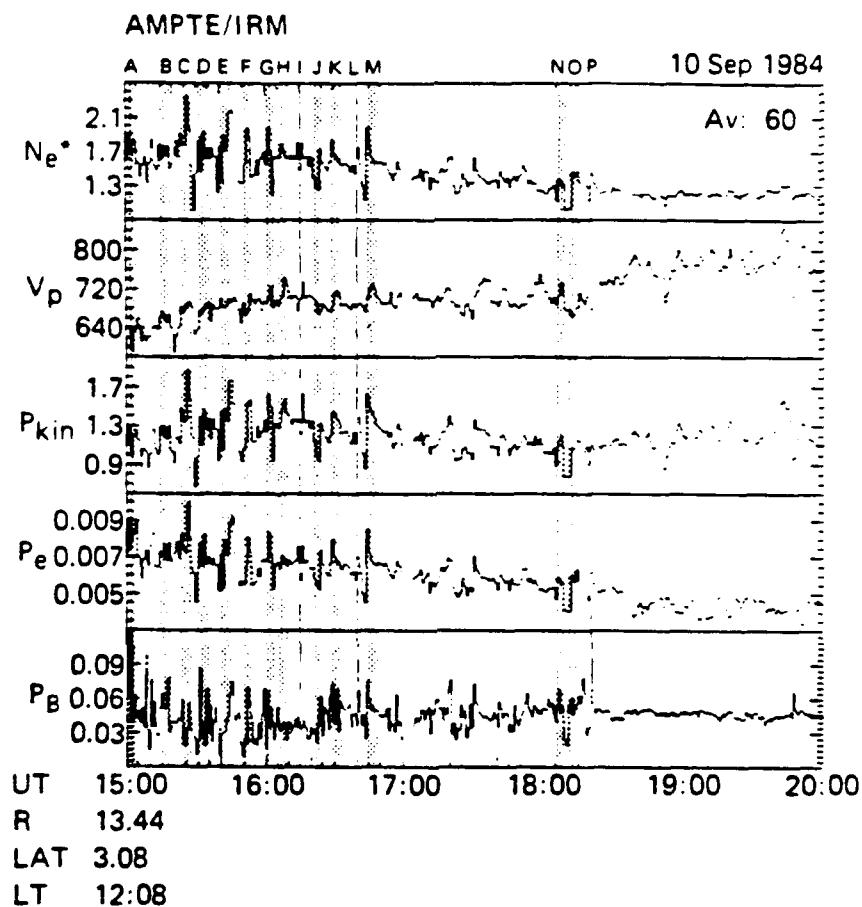
Fig. 3. AMPTE IRM Plasma and Magnetic Field (1-min average)
Measurements Upstream of the Bow Shock Indicate Quasi-
Periodic Variations in all Parameters. Density,
thermal and dynamic pressures, and magnetic field
strengths are generally in phase, so the variations
are compressional, i.e., the total pressure balance is
not maintained constant. Note the "period" (~ 8 min)
and magnitude (factor of 3) of the dynamic pressure
variations.

19

fell and its velocity rose through the interval from 1500 to 2000 UT, although there were large variations in both parameters. Variations over brief periods of 500 to 600 s contributed to a factor of 2 oscillations in the solar wind dynamic pressure, particularly from 1520 to 1600 UT. Vertical lines and letters A through P mark several of the increases in the dynamic pressure. The lines to the upper and lowermost panels demonstrate that the dynamic pressure increases were generally associated with increases in density, thermal, and magnetic pressure. The correspondence between all four parameters is quite good at 1630 (L), 1645 (M), and from 1800 to 1820 UT (N, O, P).

Figure 4 shows IRM interplanetary magnetic field (IMF) measurements averaged over 1 min for the same 5-hr interval. Early in the interval, the magnetic field pointed nearly radially toward the sun ($\theta = 0^0$, $\phi = 0^0$), but later it turned more dawnward ($\phi \sim 315^0$) and southward ($\theta < 0^0$) and the fluctuations diminished. During the interval of radial fields, IRM observed a strong upstream wave event, exhibiting amplitudes of up to 5 nT, predominantly in the transverse direction and peaking in frequency at 45 MHz. The data averaging eliminates these waves from Fig. 4, but makes the longer period variations more visible. Note in particular the strong oscillations with period ~500 s in the magnetic field strength from 1500 to 1700 UT, when the IMF was nearly radial. The compressional portion of these variations decreased from 1830 to 2000 UT, when the IMF acquired a more Parker spiral-like configuration. The amplitude of these transverse oscillations remained nearly constant.

Figure 5 shows total field measurements by each of the three satellites (IMP-8, IRM, and ISEE-2) in the solar wind during the same 5-hr interval. The IRM plot shows 1-min averages; the ISEE-2 plot contains 4-s averages; and the IMP-8 plot shows 15.36-s averages. Despite the higher time resolution, there is considerably less variation with the ~200-s period in the ISEE-2 trace than in the IRM trace. Nevertheless, some increases in magnetic field strength that we had previously associated with solar wind dynamic pressure variations at the IRM were clearly seen at

GSE DT = 60.00S

AMPTE-IRM magnetometer
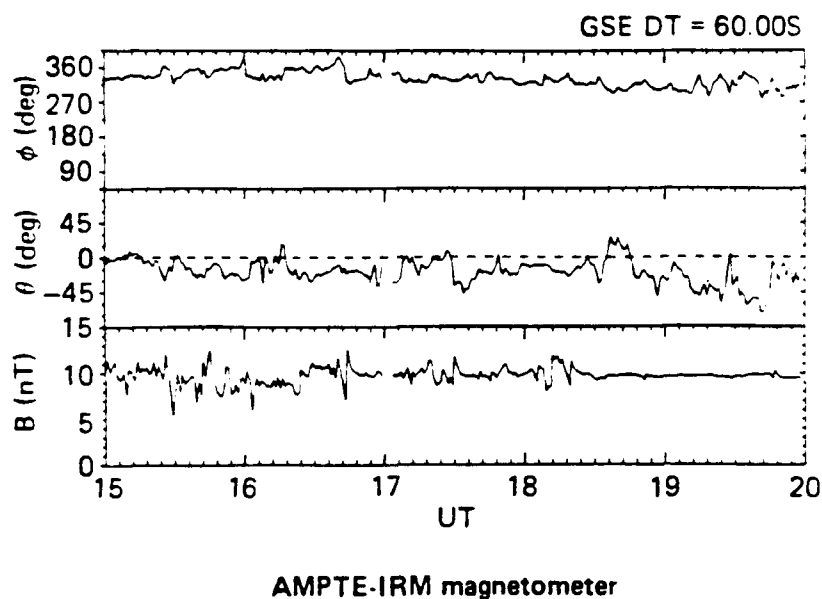
Fig. 4.   AMPTE IRM Solar Wind Magnetic Field Measurements (1-min average)
in GSE Coordinates. The IMF was nearly radial at the start of
the interval, but pointed in a typical sector direction (φ =
315°), by the end of the interval. Variations in the magnetic
field strength were greatest during the period of radial IMF.

UPSTREAM IMF
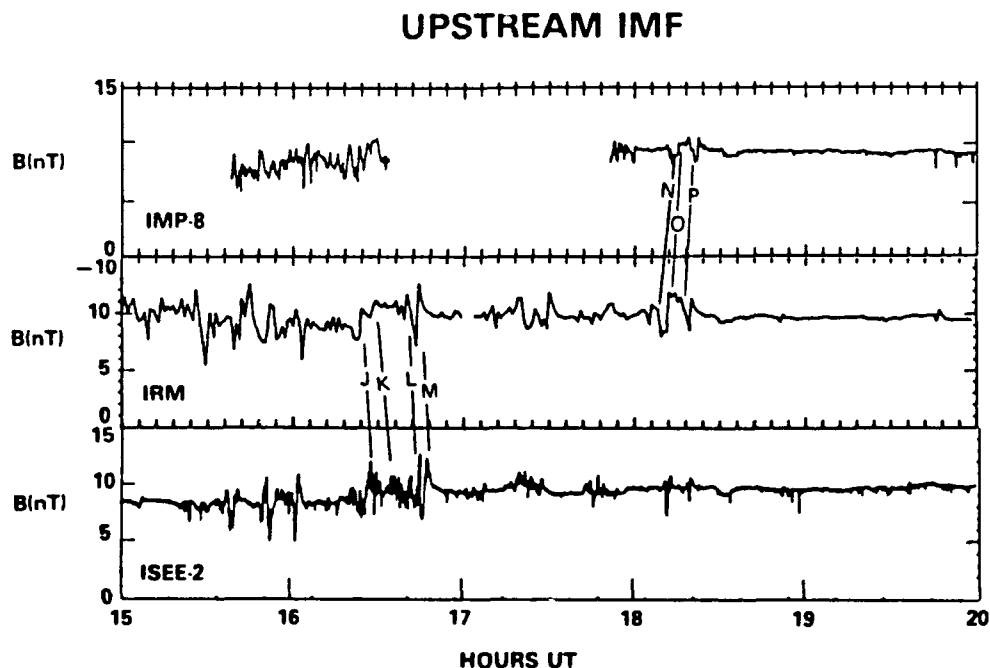
Fig. 5.   Simultaneous IMF Magnitude Observations by ISEE-2 (4-s average),
IRM (1-min average), and IMP-8 (15.36-s average). Some features
are seen at more than one satellite, but the IRM trace shows the
most variability.

21

other satellites. The IRM observed fluctuations J-M prior to ISEE-2, while the IRM observed fluctuations N-P prior to IMP-8.

The top three panels of Fig. 6 compare IRM (60-s averages), IMP-8 IOWA (2.5-min averages), and MIT (1-min averages) solar wind dynamic pressure observations from 1500 to 2000 UT. The IMP-8 plasma measurements have been normalized to standardized values according to formulae determined by King[75], but the IRM measurements have not. Previously identified solar wind dynamic pressure peaks A-P are again labeled. Although approximately 11-min period oscillations were observed in the IMP-8 IOWA data from 1530 to 1630 UT, they cannot easily be associated with any of peaks D-K identified at the IRM.

The upper two panels of Fig. 7 show 15-s averages of IRM dynamic and magnetic pressure measurements for upstream oscillations L (1640 UT) and M (1644/UT). The two traces are similar: the second peak is greater than the first, and the two are separated by a deep valley with values much less than the mean. Note the very sharp rise in the solar wind dynamic pressure by over a factor of 3 in less than a minute at the onset of peak M.

C.   MAGNETOSPHERE OBSERVATIONS

The bottom panel of Fig. 6 shows CCE magnetic field measurements in the dayside outer magnetosphere for the 5-hr interval from 1500 to 2000 UT on 10 September 1984. The average magnetic field strength decreased steadily from 1500 to 1800 UT as the spacecraft moved away from Earth. Later, as the spacecraft passed through apogee at ~1800 UT, the average field strength ceased to decrease. Variable period oscillations were superimposed upon this general trend. A comparison with the upper two panels shows that from 1500 to 1700 UT, each distinct IRM pressure pulse was followed by an increase in the magnetic field strength at the CCE location. The magnetic field strength variations were particularly large from 1520 to 1600 UT. After ~1800 UT, IRM pressure variations and CCE field observations were less well associated. The delay between IRM and CCE observations ranged from ~1 to 4.5 min and was typically ~2 min.

22
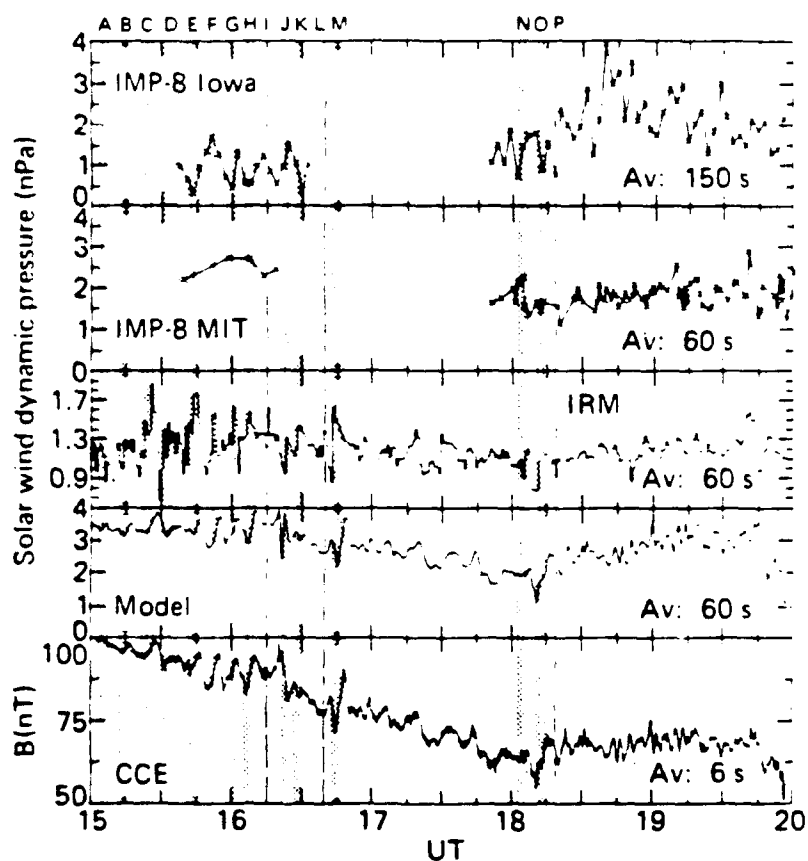
Fig. 6. An Overview of the Upstream Oscillations and Magnetospheric
Response. The top three panels compare IRM and IMP-8 obser-
vations of solar wind dynamic pressure variations. The fourth
panel shows model solar wind dynamic pressure variations
determined from the CCE observations shown in the lowermost
panel. Note that the model correctly predicts the times when
the observed solar wind pressure increases occur, but under-
estimates their amplitudes.

23
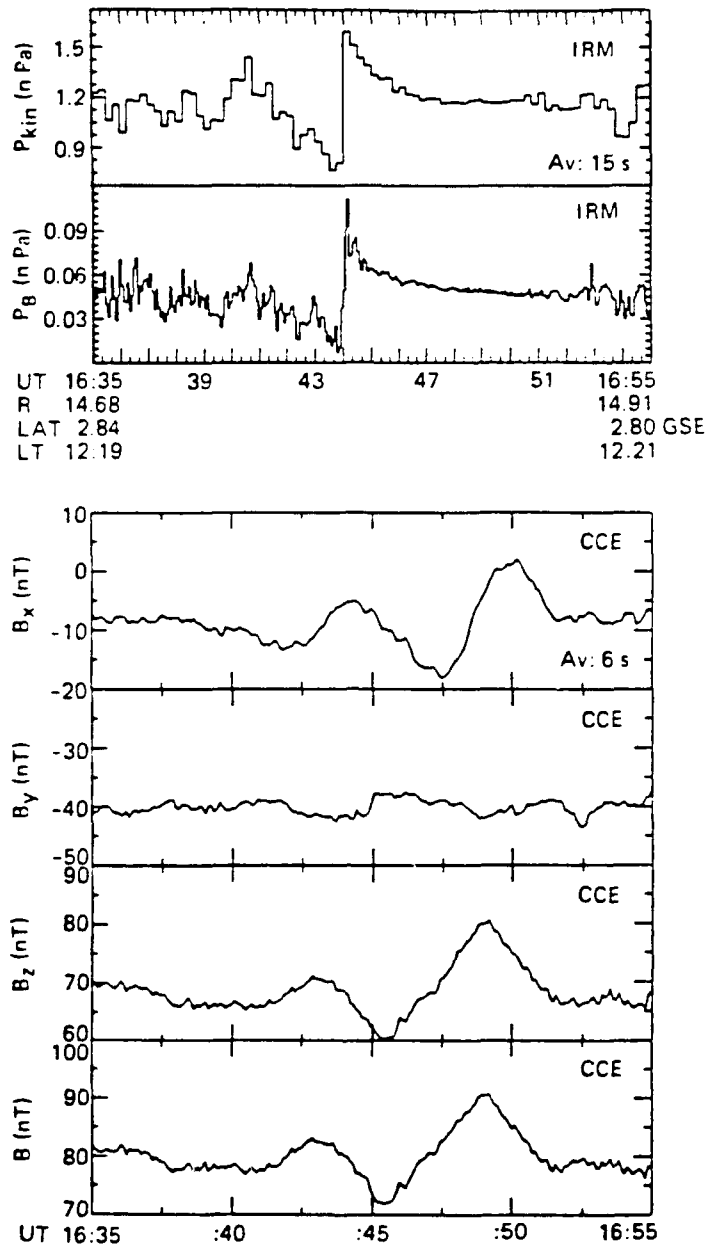
Fig. 7. High Time Resolution IRM Solar Wind Dynamic and Magnetic
Pressure Observations (15-s average) Compared to the
Magnetospheric Magnetic Field Response (6-s average) Seen
by CCE. The first two panels show that during two up-
stream oscillations the solar wind magnetic field strength
and dynamic pressure were in phase. The lower four panels
show CCE magnetic field observations of the magnetospheric
response. The B_x component becomes more negative prior to,
and more positive after, each peak in the total magnetic
field strength. This inward, outward (minus, plus) B_x
signature is consistent with southward traveling disturbances
on the magnetospause.

24

The lower four panels of Fig. 7 show high time resolution (6 s) CCE magnetospheric magnetic field observations in GSE coordinates during oscillations L and M. The main field component, B_z, and the total magnetic field strength peak at 1643 and 1649 UT. The second peak is greater than the first, and a deep depression below mean values separates them. The similarity between these features and those of the solar wind dynamic pressure trace (above) suggests a one-to-one correspondence. The first magnetospheric compression follows that upstream by ~150 s; the second by ~240 to 300 s (depending on the time chosen for the solar wind peak pressure). Note that the second magnetospheric compression is smoother than the (assumed) input upstream pressure trace: the magnetospheric magnetic field strength does not rise as abruptly.

We have run a minimum variance routine [Siscoe et al.[22]] upon the CCE magnetic field observations from 1635 to 1655 UT to determine the polarization of pulses L and M. We found the maximum variance direction to be nearly in the direction of the mean magnetic field (GSE x, y, z) = (-0.11, -0.50, 0.86), the intermediate variance direction to be nearly in the radial earth-satellite direction (0.99, 0.06, 0.16), and the minimum variance direction to be nearly in the azimuthal direction (-0.13, 0.86, 0.49). Figure 8 shows a plot of the magnetic field for this period in minimum variance coordinates, with B1 the maximum, B2 the intermediate, and B3 the minimum variance directions. The figure shows that the outer magnetospheric oscillations are nearly confined to the B1-B2 plane, i.e., the meridional plane. The transverse oscillation is therefore confined to the B2 (or radial direction).

Figure 9 compares CCE (dark) and GOES-6 (light trace) magnetospheric magnetic field observations from 1500 to 1800 UT. The compressional pulses are clearly visible in both CCE and GOES-6 traces as increases in both the total field strength and B_z. The amplitude varies more at the CCE, which is closer to the magnetopause, than at GOES-6. Note the unusual CCE pulse at 1620 UT (designated I); the magnetic field strength begins to rise, but then falls to a low value just at the time it would have been expected to
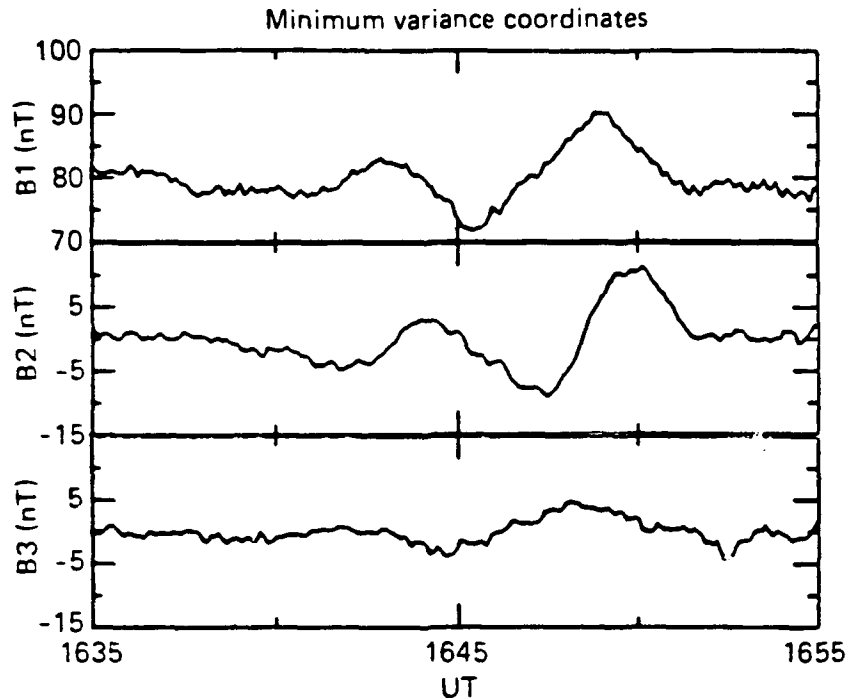
Fig. 8. A Plot of the CCE Magnetic Field Observations for the
Same Period as Fig. 7, but in Minimum Variance Coordi-
nates. B1 corresponds to the maximum variance direction,
B2 the median, and B3 the minimum variance direction.

peak. The B_z component also suddenly decreases at this time. This is the
signature expected for an incomplete, or grazing, magnetopause crossing
with a southward magnetosheath magnetic field, and indeed the external
solar wind magnetic field was southward at this time (Fig. 4). There is no
corresponding field strength increase at GOES-6 during this pulse.

Figure 10 compares CCE total magnetic field strength to the component
of the SCATHA magnetic field parallel to the model field vector expected at
the spacecraft location. A linear fit has been removed from the CCE
observations and a smooth-fit curve from the SCATHA measurements to detrend
the data, leaving only the field fluctuations. The magnetic field strength
increases at SCATHA during the 1620-UT CCE magnetopause approach. Removing
the fit fields makes apparent the presence of low-amplitude, high-frequency
variations in the magnetic fields at the CCE and SCATHA.
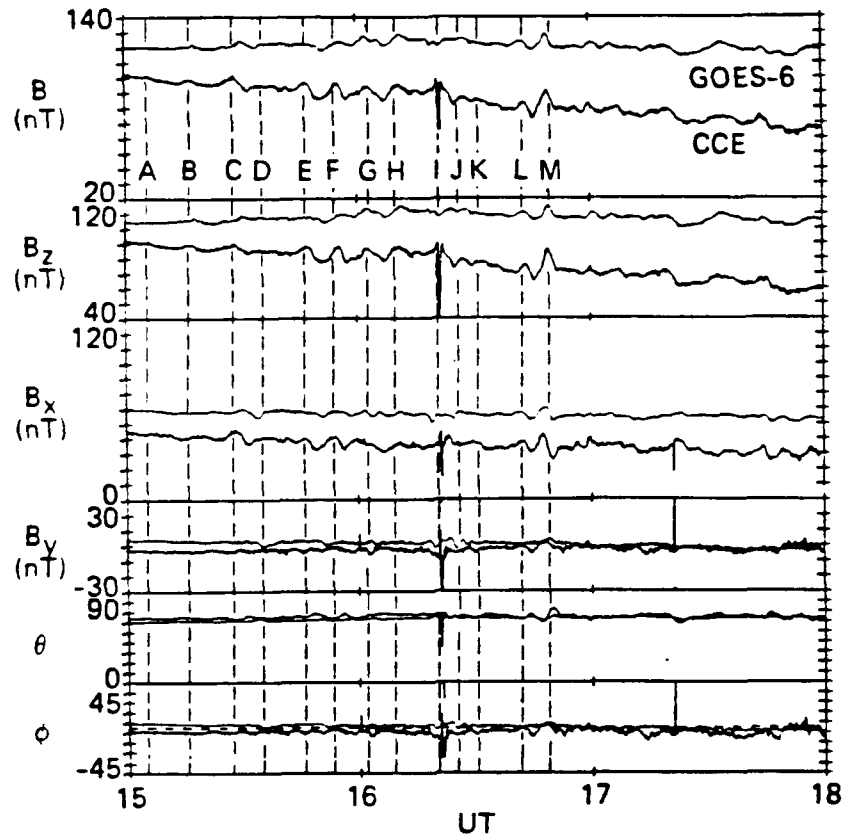
Fig. 9.   A Comparison of 6-s CCE (dark) and 3-s GOES-6 (light trace)
          Magnetospheric Field Observations from 1500 to 1800 UT.
          From top to bottom, the figure shows the total field strength,
          the three components, theta, and phi. The z axis points
          along the Earth's rotation axis, the x axis points radially
          toward Earth, and the y axis completes the right-handed
          triad. Note that magnetic field variations at both satellites
          are nearly identical, but are weaker at GOES-6.

We have examined the field strength increases observed at the CCE,
GOES-6, and SCATHA to visually determine lag times between the space-
craft. From 1500 to 1600 UT, the increases at GOES-6 lag those at the CCE
by 1 to 4 min, while those at SCATHA lag by about 1 min. From 1600 to
1700 UT, the increases at GOES-6 are more nearly simultaneous, while those
at SCATHA lead by less than 1 min.

Figure 11 shows energetic ion fluxes observed by the CCE MEPA for the
interval 1500 to 1600 UT, together with the pulse lettering system used in
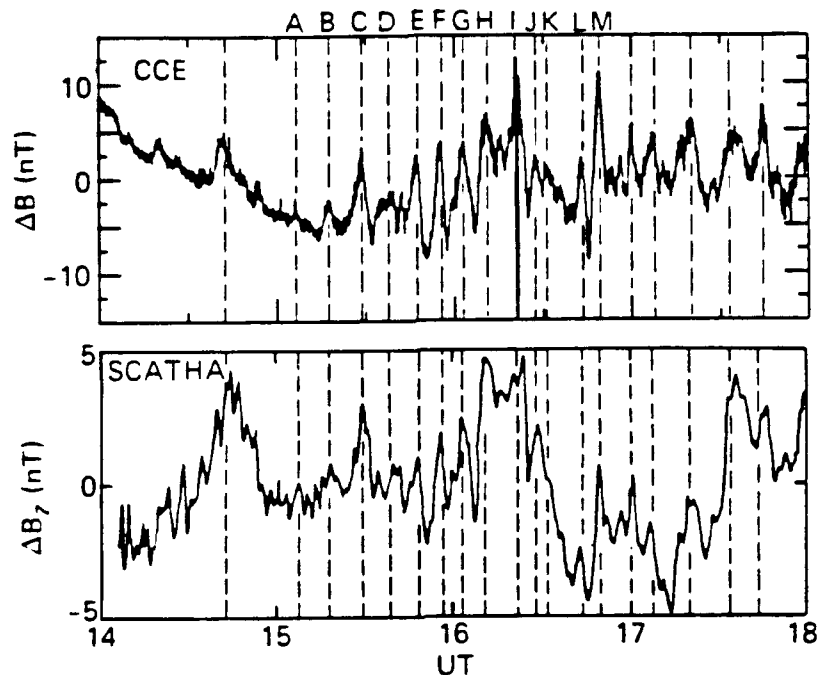
Fig. 10. A Comparison of CCE and SCATHA Magnetic Field Observations
(1-min average) from 1400 to 1800 UT. A fit magnetic field
has been determined from the CCE and SCATHA observations and
removed, so these traces show only the variations about the
mean strength. The compressional pulses in both traces
correspond well.

preceding figures. Since the spacecraft moves radially outward during this
interval, the overall particle flux decrease implies a negative radial flux
gradient over all energies that the MEPA observes. The figure indicates
that fluxes decrease over all the observed MEPA energies when the field
strength increases, and the greatest decreases occur at the highest ener-
gies. These observations are explained in the last section of the report.

D. GROUND OBSERVATIONS

Figure 12 presents measurements of cosmic radio noise absorption,
ELF/VLF emissions, and magnetic field variations obtained at the south pole
station for the 3-hr interval 1500 to 1800 UT on 10 September 1984, with
20-s resolution. The bottom panel of Fig. 12 reproduces CCE magnetic field
measurements.
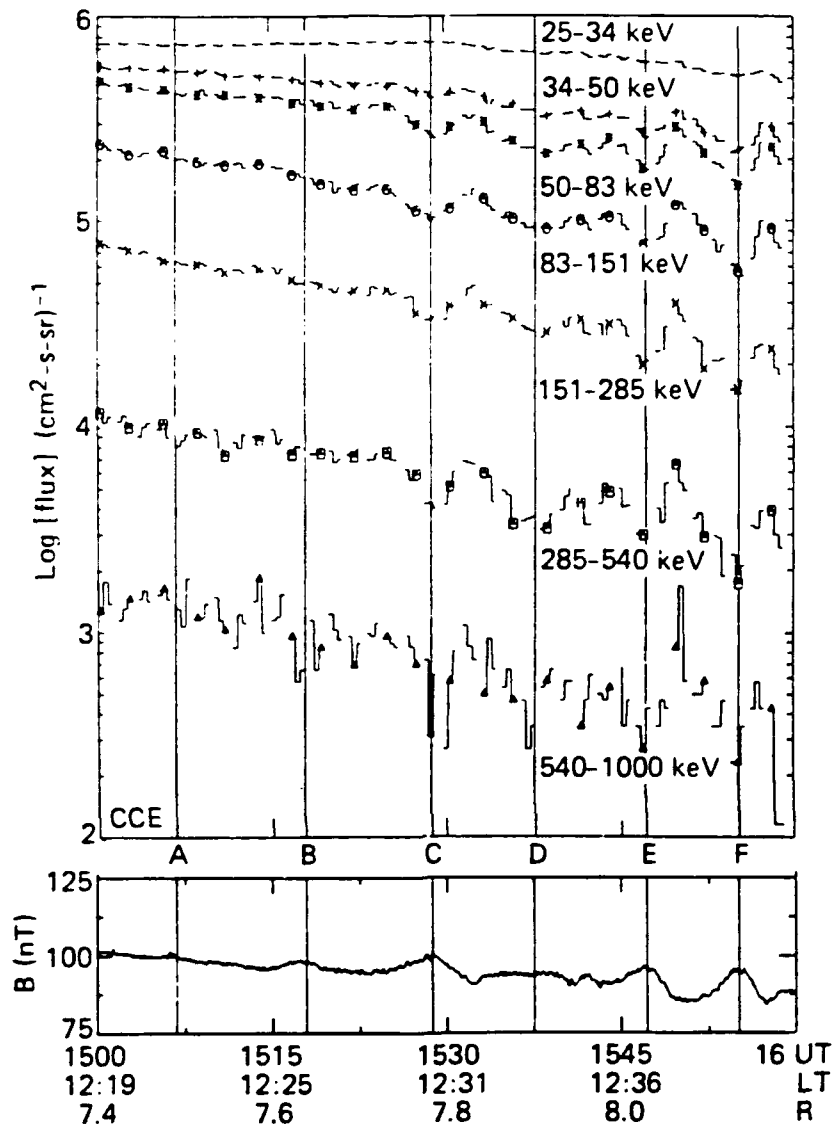
Fig. 11. A Comparison of CCE MEPA Energetic Ion Fluxes and Magnetic
Field Observations. MEPA fluxes decrease with radial
distance. Variations associated with the pulsations are
superimposed upon this pattern. The fluxes decrease when
the magnetic field strength increases.

South Pole 10 Sep 1984
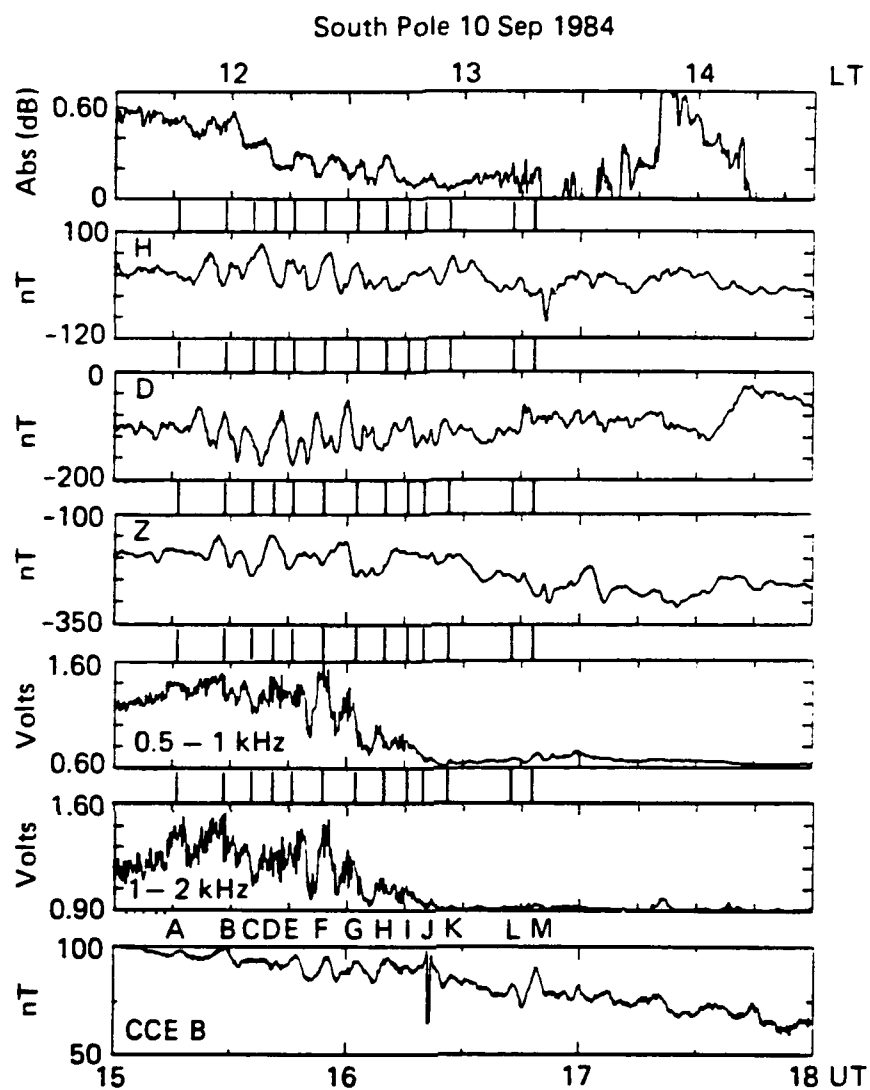
Fig. 12. South Pole Riometer (20.5 MHz), Magnetogram, and ELF/VLF
(0.1-1 and 1-2 MHz) Radiowave Emission Measurements from
1500 to 1800 UT. The CCE magnetic field strength is
shown for comparison. Vertical ticks between the panels
mark the times of peak CCE magnetic strength.

A comparison of the south pole and CCE data sets shows that a similar sequence of 8 to 10-min period oscillations was observed at both locations prior to 1700 UT. For example, relative maxima in the CCE magnetic field strength occur at or very near relative maxima in the cosmic noise absorption and H component magnetic variations, and near minima in the D component variations for most of peaks C through H, previously identified in Fig. 3. Increases in the south pole H component lag the CCE magnetic field compressions by about 1 min from 1500 to 1600 UT, and lead by less than 1 min from 1600 to 1700 UT. Such close correspondence is perhaps not too surprising, since the magnetic field lines emanating from the south pole ($\Lambda \approx 75^\circ$) near local noon would be expected to pass close to the subsolar magnetopause and thus to CCCE.

Power spectra calculated for the south pole magnetic field variations showed a peak in the period range ~8 to 10 min. Figure 13 shows the three vector components of the south pole magnetic field filtered in the band 8 to 10 min. The enhanced wave activity during the last half of hour 15 is clearly evident, as is additional activity, particularly in the vertical (z) component following hour 17.

The polarization characteristics of the magnetic field vector in the H-D plane are presented as hodograms covering the period 1524 to 1614 UT in Fig. 14. The data have been filtered in the band 480 to 600 s prior to plotting. The field vector rotates in the counter-clockwise direction (CCW), which corresponds (for the southern hemisphere observations) to a right-hand (RH) polarization. Statistically, this is the expected polarization sense for a surface wave observed in the local afternoon sector [Atkinson and Watanabe[38]].

Each magnetosphere compression presumably propagates to the ground as a compressional MHD wave, giving rise to the observed ground magnetic signature. The small (~0.2 dB) riometer absorption pulses are a manifestation of enhanced D region ionization produced by precipitating electrons with energies U ≥ 10 keV. The association of the absorption pulses with the magnetospheric magnetic field compressions observed by CCE indicates

31

SOUTH POLE FILTER 8-10min.

H | 10nT

D | 10nT

Z | 10nT

15   16   17   18

10 SEPTEMBER 1984
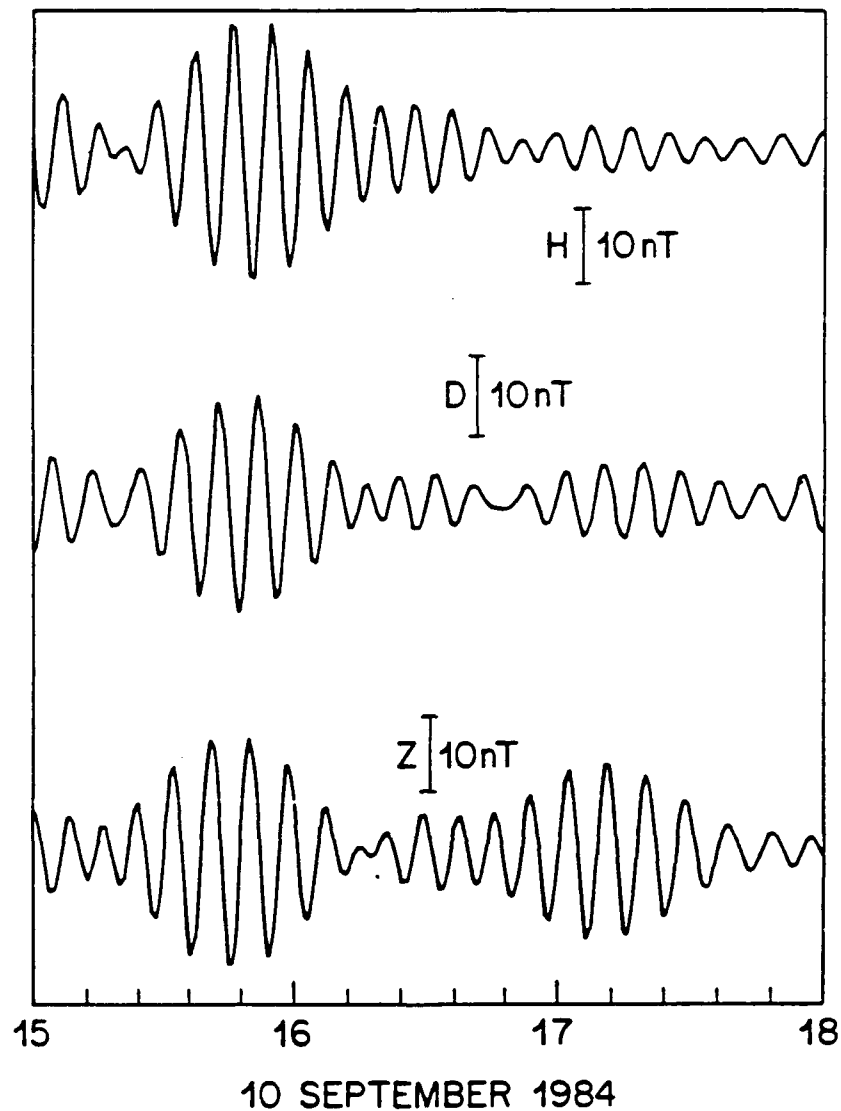
Fig. 13. South Pole Magnetogram Measurements Filtered to Show 8 to
10-min Variations During the Period from 1500 to 1800 UT

that the field compressions have perturbed the quasi-trapped electron
population, causing small fluxes of electrons to be lost to the atmo-
sphere. As can be seen in Fig. 12, these weak precipitation enhancements
are superimposed on a slowly decreasing absorption (i.e., precipitation)
level.

SOUTH POLE
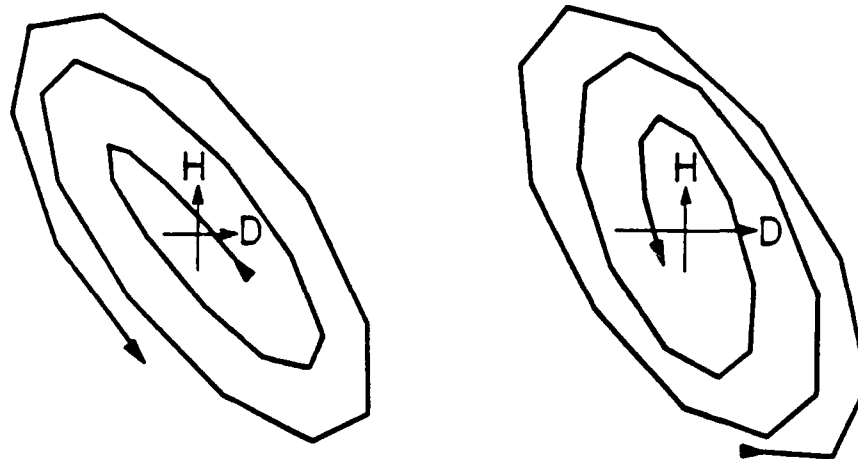
1525-1548 UT   1549-1613 UT

10 SEPTEMBER 1984

Fig. 14. Hodograms of South Pole Magnetograms for the
          Period from 1524 to 1614 UT Indicate the
          Presence of Right-Hand Polarized Waves

The intensity of ≤ 2 kHz emissions recorded at the south pole
between 1515 and 1615 UT also exhibited modulations like those of the
riometer absorption in this interval. Amplitude modulations were observed
in the 0.5-1 kHz and 1-2 kHz channels, as shown in Fig. 12. None of the
higher frequency bands exhibited these modulations. The observed ELF/VLF
activity is expected to have been generated in one or more source regions
located near the equatorial plane within the viewing region and to have
propagated to the ground in field-aligned ionization ducts [e.g.,
Helliwell[76]]. Since ground-based ELF/VLF receivers observe signals exiting
ducts as much as 1000 km away from the station [Walker[77], Tsuruda et
al.[78]], the viewing area of the south pole probably included much of the
dayside portion of the outer magnetosphere during the period of these
observations--a region considerably larger than that monitored by either
the riometer or magnetometer. The propagation restrictions that generally

33

limit ducted waves to frequencies below half the equatorial gyrofrequency [Helliwell[79]] provide a method for identifying the radial position of the wave source region, but the 1 to 2-kHz upper cutoff frequency in this event is consistent with a source region at any radial distance inside the esti- mated magnetopause boundary given by $R_s = 8.5\ R_E$. The wave amplitude at the south pole maintained relatively identifiable oscillations with ~500-s periods for a duration of about 30 min, suggesting either that the number of contributing source regions was small or that the dominant source regions were modulated at similar frequencies and phases.

IV. INTERPRETATION

In this section we consider the nature of the upstream solar wind
dynamic pressure variations, the relationship between the pressure
variations and the compressional magnetospheric signatures, and the cause
of the signatures seen at high latitudes on the ground.

A.   SOLAR WIND

We consider two possible sources for the large-amplitude, short-period
solar wind dynamic pressure variations intrinsic to the solar wind and
generated at the bow shock. Neither suffices to explain all the observa-
tions, but we somewhat favor the bow shock source. Consistent with this
source, the observations were strongly compressional, occurred only during
the period of radial IMF, and were strongest at the IRM, the spacecraft
closest to the quasi-parallel bow shock. The compressional variations that
were observed are a common feature of the quasi-parallel shock, but have
only been reported with shorter periods. Furthermore, the lack of correla-
tion between the IRM solar wind dynamic pressure variations and those seen
at IMP-8, as shown in Fig. 6, suggests that the upstream dynamic pressure
variations were a local phenomena generated at the bow shock. These points
are inconsistent with the solar wind source. In particular, it is diffi-
cult to understand what process could produce and maintain such strong
pressure variations in the ambient solar wind.

However, other features of the upstream oscillations are less easy to
reconcile with a bow shock source. First, oscillations with periods
of ~8 min have never been reported in this region. Although Spangler
et al.[31] reported two instances of density wave packets with periods of 4
to 5 min upstream of the quasi-parallel bow shock, the high time resolution
plots shown in our Fig. 7 do not suggest modulation of shorter (< 1 min)
waves as the source of our pressure variations. In addition, some magnetic
field signatures associated with the pressure variations were seen at more
than one upstream satellite, and they produced a single repeatable

magnetospheric response. Timing considerations at the three upstream
satellites may be consistent with a solar wind source for the upstream
pressure variations. The upstream magnetic field fluctuations (N-O) were
observed by IRM prior to IMP-8 (Fig. 5) during a period of spiral IMF
(Fig. 4), consistent with the delay expected for solar wind features moving
past the spacecraft. However, fluctuations J through K were seen at IRM
shortly prior to ISEE-2 during a period of nearly radial IMF. It is less
clear that these delays are consistent with the advection of solar wind
variations. These observations suggest a great spatial extent for the
phenomena and are not consistent with a bow shock source. Perhaps the
observations required intensification of pre-existing solar wind features
at the quasi-parallel shock.

B. MAGNETOSPHERE

The multispacecraft magnetospheric magnetic field observations indi-
cate that quasi-periodic, ~8-min period, magnetic field variations occur
throughout the dayside magnetosphere. In general, the quasi-periodicities
could be directly associated with the upstream pressure variations,
triggered by a single sharp change in upstream pressure, or be completely
unrelated.

We have ruled out the possibility that the magnetospheric oscillations
are completely unrelated to the upstream pressure variations (i.e., that
they are due to some wholly internal magnetospheric process) since we are
able to establish an almost one-to-one correlation between solar wind
dynamic pressure variations and fluctuations in the magnetospheric magnetic
field during the period from 1500 to 1700 UT. It would be very unlikely
for the upstream solar wind and magnetosphere to oscillate simultaneously
with similar periods if driven by different sources. On similar grounds,
we also rule out the possibility that single, sharp, solar wind pressure
pulses set off a series of geomagnetic oscillations. No such solitary
peaks were observed in the solar wind.

We do not consider FTEs or magnetopause boundary waves driven by the Kelvin-Helholtz instability to be the cause of the magnetospheric oscillation, since these would be unrelated to the upstream pressure pulse. The similarity of the magnetospheric oscillations at each magnetospheric satellite and their association with upstream solar wind pressure variations argue against the magnetospheric oscillations being produced by a series of FTEs and/or boundary waves. Nor does it seem likely that the upstream variations could excite magnetospheric oscillations at similar frequencies over the wide range of local times and L shells.

The magnetospheric observations are consistent with, and best explained by, a series of upstream solar wind dynamic pressure pulses. Each upstream pressure pulse should have a similar and distinct effect upon the magnetosphere, and, indeed, each could be associated with a brief magnetospheric compression seen at the three satellites in the dayside magnetosphere. However, the increases in the upstream solar wind dynamic pressure do not last long enough for the dayside magnetosphere to be brought into equilibrium. Thus, the pressure increases should each produce single tailward-propagating troughs in the magnetopause position which appear as tailward-propagating surface wavelets. The CCE magnetic field oscillations are consistent with the passage of southward-moving boundary ripples: the magnetic field turns inward ($-B_x$), is compressed, and turns outward ($+B_x$) as the trough of a ripple passes, consistent with the conceptual model shown in Fig. 1.

The lag times suggest that the upstream pressure pulses first struck the postnoon magnetopause. When the CCE was the only observing station in the postnoon region, it invariably recorded magnetic field strength increases first. As other spacecraft moved into the postnoon region, CCE lead times diminished, and some compressions were observed earlier at SCATHA, GOES-6, and the south pole. The compression at 1620 UT caused a brief CCE magnetopause crossing, but was not observed at GOES-6, perhaps indicating that it alone was caused by a small-scale localized solar wind feature. However, we note that a compression was observed at this time at

37

SCATHA. The upstream pressure variations and the magnetospheric response were less well correlated after 1700 UT, as all the satellites moved away from local noon.

If, as we have suggested, the upstream pressure variations with ~500-s periods were generated at the quasi-parallel bow shock during an interval of radial IMF, then they should more commonly be found upstream of the dawn bow shock for a normal spiral IMF. Furthermore, the pulses should be swept tailward through the dawn magnetosheath and drive greater amplitude dawn than dusk magnetopause motion. Observations consistent with these predictions have already been reported. Heacock and Chao[80] reported simultaneous magnetosheath and ground magnetogram observations. Their Figure 5 shows the onset of ~4-min period oscillations in the polar magnetosheath magnetic field strength and in several high-latitude ground magnetograms at 2215 UT on 4 October 1974. In our model, the magnetic field oscillations in the magnetosheath would be associated with dynamic pressure variations driving magnetopause motion and the oscillations observed at the ground. Observations reported by Tsurutani et al.[81] more directly demonstrate the relationship between magnetosheath magnetic field and plasma variations. They noted a single case of simultaneous IMP-8 near-Earth and ISEE-3 distant magnetosheath observations that indicated the presence of magnetic field and plasma oscillations with quasi-periods of ~6 min in the distant magnetosheath, but their absence nearer Earth. The oscillations were therefore generated either at the downstream bow shock or in the distant magnetosheath. The most interesting characteristic of these oscillations was an in-phase variation of the plasma density and magnetic field strength, rather like the variations that the IRM observed upstream of the bow shock in this study. We assert that the compressional magnetosheath oscillations observed by Heacock, Chao, and Tsurutani et al. are the downstream manifestation of the upstream solar wind oscillations indicated in this report. The statistical study of Howe and Siscoe[82] indicates greater amplitude dawnside magnetotail magnetopause motion than duskside, consistent with the prediction for magnetopause motion driven by pressure variations generated at the quasi-parallel bow shock.

We have also seen that the energetic ion flux at the CCE oscillated in response to the magnetospheric compressions: the flux minima correspond to peak magnetic field strengths. The oscillations were superimposed upon a radial flux gradient, and flux levels returned to these values when no oscillations were present. This suggests that the flux variations can be modeled adiabatically (see below).

C.   GROUND STATION

Anger et al.,[83] Barcus and Rosenberg,[24] and Samsonov et al.[84] have previously reported an association between long-period (300 to 360 s) pulsations in electron precipitation, hydromagnetic waves, and ELF/VLF radiation at dayside high latitudes similar to those shown in Fig. 12. Walker et al.[85] determined that some sort of magnetopause boundary motion was required to produce the 600-s period oscillations that they observed in ionospheric plasma velocities. Some or all of these oscillations could be directly related to solar wind pressure-driven magnetospheric compressions. Again, our proposed quasi-parallel bow shock origin for the driving dynamic pressure pulses and the typical spiral IMF suggest a greater occurrence rate for long-period pulsating-ground riometer observations, pre- rather than postnoon, as reported by Barcus and Rosenberg[24].

The correlation between the riometer absorption pulses and ELF/VLF activity at the south pole indicates that the precipitation mechanism involves a wave particle interaction between the magnetosphere electrons and ELF/VLF waves. A similar process was proposed [e.g., Perona[86]] to explain electron precipitation that is observed during some sudden impulses and sudden commencements [e.g., Brown[87,88]], events that are also driven by variations in solar wind pressure. Gail[89] and Gail et al.[90] studied a number of SSCs in detail. They concluded that the commonly observed wave-growth enhancement and the increased probability of triggering discrete emissions resulted directly from the SSC magnetic field compression and that the electron precipitation was due to increased scattering by the waves.

Finally, we note that the amplitudes of the 500 to 600-s variations observed at the upstream IRM (Fig. 3), the magnetospheric CCE (Fig. 10), and at the south pole station on the ground (Fig. 12), all reached their greatest amplitudes during the period from 1520 to 1600 UT, further indicating a direct upstream pressure variation source for the magnetospheric oscillations.

V. MODEL RESULTS

A. PREDICTING SOLAR WIND PRESSURE FROM MAGNETOSPHERIC OBSERVATIONS

If solar wind pressure variations are the direct cause of the compressions observed in the magnetospheric magnetic field, it is interesting to determine to what extent upstream variations can be predicted from observations made inside the magnetosphere. We study this by combining two simple models of the dayside magnetopause.

Chapman and Ferraro[91] adopted an image dipole model to determine the "magnetopause" location. Their model assumes that an infinite current sheet in the plane transverse to the solar wind flow separates that flow (which is brought to a rest) from the Earth's magnetic field. Currents in the plane both shield the solar wind from the Earth's magnetic field and increase the magnetic field strength throughout the region in which the Earth lies. The increased magnetic field strength on the earthward side of the boundary can be modeled as the sum of the fields due to the Earth's dipole and an image dipole, with the latter located sunward of the plane on the Earth-sun line at the same distance from the boundary as the Earth, which lies behind the plane.

Martyn[92] suggested that the equatorial boundary between the Earth's magnetic field and the solar wind stream lies at the point where the solar wind dynamic pressure balances the magnetic pressure just inside the magnetopause hollow. The pressure balancing approach to predicting the magnetopause position succeeds because the dynamic pressure greatly exceeds the plasma thermal $[nK(T_i + T_e)]$ and magnetic $(B^2/2\mu_0)$ pressures in the solar wind [e.g., King[93]], and this dynamic pressure is converted into a proportional thermal pressure just outside the subsolar magnetopause [Landau and Lifshitz[94]]. The magnetic pressure generally dominates the other two in the magnetosphere, although thermal and magnetic pressures are comparable at times in the boundary layer [e.g., Paschmann et al.[95]].

The important point here is that one may combine the models of Martyn and of Chapman and Ferraro to determine the magnetopause location and solar wind dynamic pressure from magnetospheric magnetic field measurements alone. More complicated models can be considered [e.g., Olson and Pfitzer[96]], but are not required for our purposes.

Figure 15 illustrates the image dipole model used to predict the magnetopause location and upstream solar wind dynamic pressure from CCE magnetospheric magnetic field observations. This simple model contains the first-order effects that we seek despite the fact that it is formally valid only near the subsolar magnetopause and for no dipole tilt. As the observations were made in September, near the equinox, the latter assumption is safe. The magnetic field strength (B) in the magnetosphere is given by the sum of the Earth's dipole field (B_d) and that of the image dipole of equal strength which lies equidistant from the magnetopause [Hess[97]]

$$B = B_d/R_d^3 + B_d/R_i^3 \qquad (1)$$

One feature of Eq. (1) is that the magnetic field strength at any point on the magnetopause is twice as great as that of the Earth's dipole alone.

When it is limited to the ecliptic plane, Eq. (1) can be solved for R_s, the distance from Earth to the subsolar point

$$R_s = 0.5 \ \{[(B/B_d - 1/R_d^3)^{-2/3} - Y^2]^{0.5} + X\} \qquad (2)$$

Since the position of the observing spacecraft, $R_d^2 = (X^2 + Y^2)$ with all quantities in R_E, is a known function of time, only the time history of the observed magnetospheric magnetic field strength (B) is required to find R_s. Once R_s is known, the magnetic field strength just inside the subsolar magnetopause can be determined, $B_s = 2B_d/R_s^3$. From this quantity one learns the time variation of the solar wind dynamic pressure, given by $B_s^2/2\mu_0$.
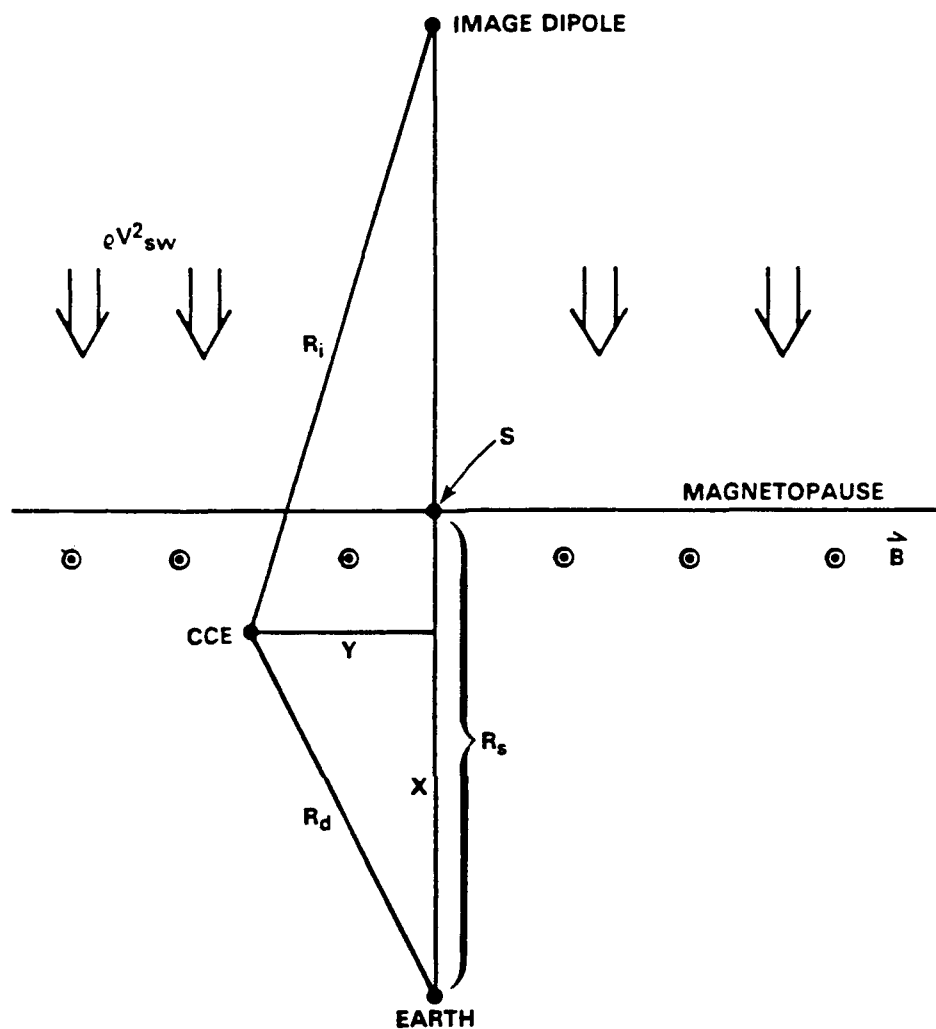
Fig. 15. The Image Dipole Model in the Ecliptic Plane. The image
dipole lies along the Earth-sun line and has the same
strength as the Earth's dipole, so their combined strength
at the magnetopause is twice as great as that of the Earth's
dipole. An observing spacecraft is located at point CCE,
a distance y from the Earth-sun line, a distance R_d from
the Earth's dipole, and a distance R_i from the image dipole
The distance to the subsolar magnetopause is given by R_s.

43

The magnetic field strength observed just inside the 1620 UT magneto-
pause crossing proves useful in normalizing Eq. (1). We found that the
greatest 6-s average field strength just inside the magnetopause was
98.5 nT. Combining this with our knowledge of the spacecraft position
(X_{GSE} = 8.081, Y_{GSE} = 1.763 R_E) at this time, and the fact that R_d = R_i at
this point, we can solve for B_d. This effective B_d(= 27866 nT) differs by
10% from that of a dipole, in part due to our assumption of a planar
boundary and, in part, to missed plasma pressure contributions to the
magnetospheric pressure.

Figure 16 shows traces of the subsolar magnetopause location, subsolar
magnetospheric magnetic field strength, and solar wind dynamic pressure
derived from 1-min averaged CCE magnetospheric magnetic field observa-
tions. We predict magnetopause motion from 1500 to 1700 UT with an
amplitude of about 0.2 R_E and a quasi-period of ~500 s, similar to the
motion reported by Williams[98].

Figure 6 compares model and observed IRM solar wind dynamic pres-
sures. The solar wind pressures predicted from CCE observations are about
twice as great and generally occur several minutes later than those
observed upstream at the IRM. Although the model overestimates the mean
solar wind dynamic pressure, it does correctly predict the amplitude of the
solar wind variations: both the observed IRM solar wind pressure and the
pressure predicted from magnetospheric observations vary by about 1 nPa.
The magnetosphere was unable to respond to the shortest period variations
since the solar wind pressure pulses do not last long enough to establish a
stable pressure balance between the solar wind and magnetosphere. Several
minutes are required for this balance to be established [Baumjohann
et al.[9]].

B. PREDICTING THE MAGNETIC FIELD STRENGTH AT GEOSYNCHRONOUS ORBIT

Roederer[99] provides a simple empirical model for the equatorial
geomagnetic field strength in the range 1.5 < r < 7 R_E as a function of the
radial distance from the Earth to the subsolar point on the magnetopause.
His model predicts that
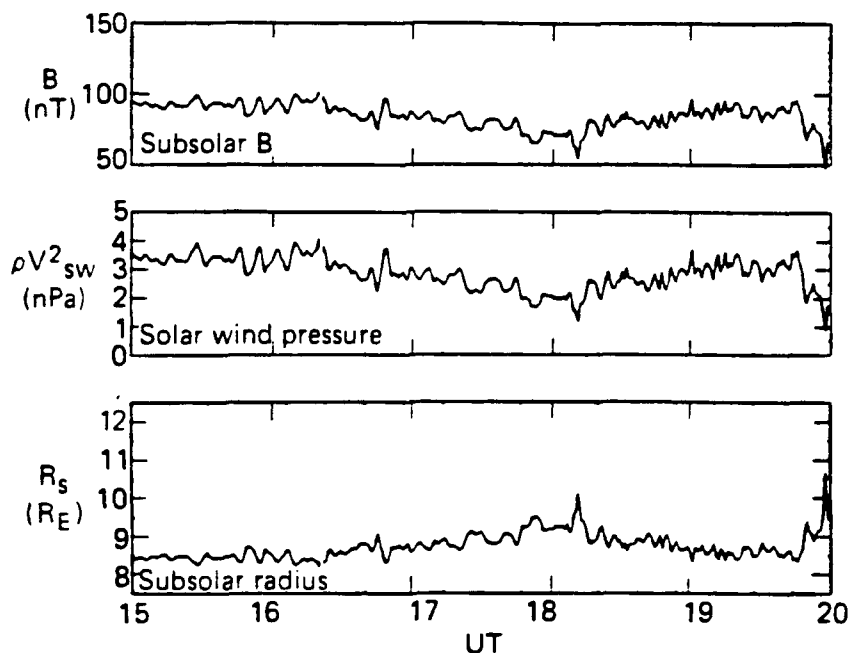
Fig. 16. Results of the Image Dipole Model. The Top Panel Shows a
Trace of the Predicted Subsolar Magnetospheric Magnetic
Field Strength, the Middle Panel Shows the Predicted Solar
Wind Dynamic Pressure, and the Lower Panel Shows the Pre-
dicted Subsolar Radius.

$$B = k_0/r^3 + k_1 - k_2 r \cos\phi \tag{3}$$

where

$$k_0 = 31100 \text{ nT } R_E^3$$

$$k_1 = 12(10/R_s)^3 \text{ nT}$$

$$k_2 = 2.27(10/R_s)^4 \text{ nT } R_E^{-1}$$

Here (r, ϕ) is the observer's position, with r measured in R_E and ϕ in
longitude east of midnight. The subsolar magnetopause lies at R_s. We
know (r, ϕ) from GOES-6 ephemeris, and we estimate the subsolar magneto-
pause position (R_s) from Eq. (2) and Fig. 16. Thus, we can predict the
magnetic field that GOES-6 should observe and compare it with that actually
observed. Figure 17 shows the results of this comparison. Clearly, the

45

magnetopause position (R_s) from Eq. (2) and Fig. 16. Thus, we can predict the magnetic field that GOES-6 should observe and compare it with that actually observed. Figure 17 shows the results of this comparison. Clearly, the predicted and observed compressions are nearly time coincident. The predicted magnetic field strengths are too great by a constant value throughout the interval (consistent with our overestimate of the solar wind dynamic pressure above), but the predicted and observed variations have nearly identical amplitudes. The successful comparison between predicted and observed GOES-6 magnetic field strength traces indicates that it is possible to predict the magnetic field strength at one magnetospheric satellite from another. Further, the process could have been reversed. We could have used geosynchronous magnetic field observations (offset by a constant) to predict the magnetopause location and variations in solar wind dynamic pressure [Sauer and Rufenach[100], Olson and Pfitzer[96]].
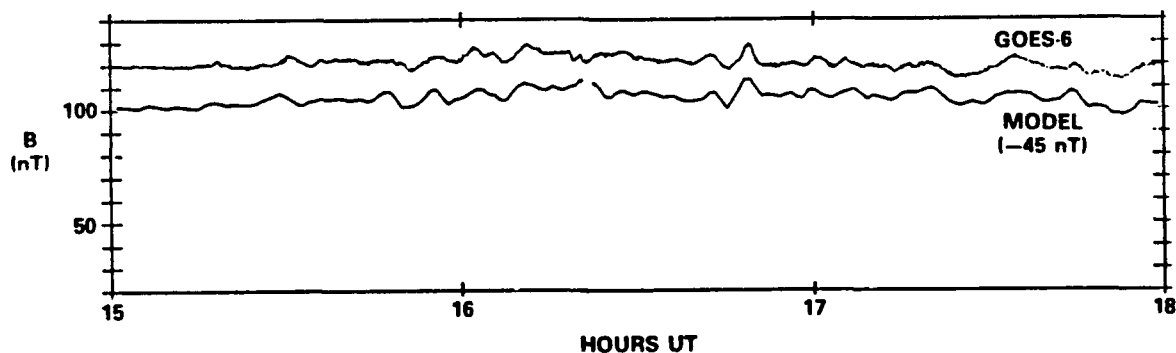

Fig. 17. A Comparison of the Predicted and Observed Magnetic Fields at the Position of GOES-6. The traces are nearly identical except that predicted strengths are uniformly greater by a constant value.

C. PREDICTING ENERGETIC ION FLUX VARIATIONS DURING COMPRESSIONAL OSCILLATIONS

The energetic ion flux decreases associated with the magnetic field compressions observed at CCE can be modeled using a technique originally outlined by Konradi[101], and later used by Wilken et al.[10] to model energetic magnetospheric particle flux variations attending an SSC. Here "sudden" is rapid in comparison with ion drift periods, which are of the order of 2 hr for 100-keV protons at L = 9 in a compressed magnetosphere [Sibek et al.[102]]. The oscillations shown in Fig. 11 clearly satisfy this condition. As Wilken et al.[10], we will assume that the magnetospheric spectra can be fit by a power law

$$j(T,R) = k(R)T^{-\gamma(R)} \tag{4}$$

with j being the ion differential flux, T the ion energy, R the radial distance from Earth in R_E, and $k(R)$ and $\gamma(R)$ the spectral parameters. They further assumed a separable, constant flux dependence upon pitch angle and the validity of Eq. (4) over energies above and below those observed by the spacecraft. With these assumptions, Wilken et al. found a first-order linearized equation for flux variations during a magnetospheric compression

$$\delta j/j(T) = \delta B/B_o (\gamma_o + 1) + \delta k/k_o + \delta_\gamma/\gamma_o \ln(j_o/k_o) \tag{5}$$

All quantities with subscript o are to be measured further radially outward in the magnetosphere than the CCE location, at the position of the particles and field lines prior to the compression that transports them to the CCE location. The third and perhaps second adiabatic invarients are violated during the compression. The first term on the right of Eq. (5) represents adiabatic energization; the latter two terms together describe the radial flux gradient. Unlike Wilken et al., who used data from geosynchronous satellites, we have direct measurements of the flux as a function of radial distance from CCE observations (assuming no flux changes during the CCE sampling time over the radial distance). We use Eq. (5) to compare

47

observed and predicted flux decreases during the magnetospheric compressions. First, we recognize that the sum of the latter two terms in Eq. (5) must be negative for each energy in our case, since the radial flux gradient for all energies shown in Fig. 11 is negative. The first term in Eq. (5) is positive for a compression. Consequently, the observed flux at a spacecraft location falls during a compression when the sum of the latter two terms exceeds the former. However, note that the flux on a field line rises during compressions for any spectra with a positive spectral index γ.

We have fit power laws Eq. (4) to the spectra observed at 5-min intervals from 1500 to 1520 UT on 10 September 1984, corresponding to spectra at radial distances of 7.43 to 7.74 R_E from Earth, and for the energy range of 25 to 540 keV. We then determined the radial flux gradients of k and γ. The results obtained indicated that the power law fit as a function of radial distance at this time and location could be well described by

$$ j = 10^{-3.81 + 1.66 R} T^{5.71 - 1.12 R} \tag{6} $$

Returning to Eq. (5), with typical values observed during the period 1500 to 1600 UT, $\delta B = 5$ nT, $B_0 = 92$ nT, $R = 0.2 R_E$, $\gamma_0 = 2.75$, and $R = 7.56 R_E$, we find

$$ \delta j/j_0 = 0.968 - 0.224 \ln(T) \tag{7} $$

Equation (7) predicts an increase in the CCE flux at lower energies and a decrease at higher energies, with the separation energy near 75 keV. In one respect, Eq. (7) agrees well with the observations. The observed decreases are greatest for the highest energy channels. However, the MEPA observed no flux increase during the compressions for energies below 75 keV. At best, the fluxes at lowest energies remained nearly constant. Thus, it appears that one or more model assumptions were violated. We examined high-resolution pitch angle distributions (PADs) during this interval and found that they were a function of energy. PADs for ions with

energies 25 to 34 keV had relative flux minima at pitch angles near 90°, but those ions at higher energies had strong flux maxima at pitch angles near 90°. One of the model assumptions was similar pitch angle distributions at all energies; the violation of this assumption may be the cause for the false prediction of an increasing low-energy flux during the compressions.

VI. CONCLUSIONS

In this report, we have emphasized the existence of strong quasi-periodic oscillations in the solar wind plasma and magnetic field just upstream of the bow shock. Pressure balance within the solar wind is not maintained during the oscillations; rather, the solar wind thermal and magnetic pressures generally varied in phase. The solar wind dynamic pressure varied at times over a factor of 3 during the oscillations. We infer that these changes were transmitted through the magnetosheath to the magnetopause, where they generated magnetopause boundary wavelets. The local magnetopause and magnetosphere responded to each variation, contracting when the solar wind dynamic pressure increased and expanding when it decreased. The boundary wavelets should move tailward with the magnetosheath flow.

The solar wind pressure variations were directly associated with compressional oscillations in the magnetic field observed at each of several satellites located in the dayside magnetosphere. The results of our modeling indicate that even brief variations in solar wind dynamic pressure can be successfully monitored by satellites located at geosynchronous orbit or beyond. However, the magnitude of the upstream variations will be underestimated, since the magnetosphere never fully responds to brief solar wind inputs. We also found that the pressure oscillations can drive quasi-periodic variations in the energetic ion flux in the dayside magnetosphere. The sense and magnitude of these variations can be estimated when the radial flux gradient and magnetic field variations are known. It will be necessary to include the variation of ion pitch angle with energy to achieve more quantitative results.

The magnetosphere compressions apparently also perturbed the magnetosphere electron fluxes, causing electron precipitation pulses and small enhancements of the D region ionization at high latitudes. Finally, variations in the geomagnetic field with similar periods were seen at the

51

high-latitude south pole station. Although we could not always associate these oscillations in a one-to-one manner with those in the solar wind, we suggest that upstream solar wind pressure oscillations produce magnetopause surface waves that, in turn, drive some observations of high-latitude ground pulsations with periods of ~10 min.

REFERENCES

1. Yumoto, K., "External and Internal Sources of Low-Frequency MHD Waves
    in the Magnetosphere--A review," J. Geomag. Geolec., 40, 292-311
    (1988).

2. Kaufmann, R. L. and A. Konradi, "Explorer 12 Magnetopause Observa-
    tions: Large-scale Nonuniform Motion," J. Geophys. Res., 74,
    3609-3627 (1969).

3. Gosling, J. T., et al., "Measurements of the Interplanetary Solar
    Wind During the Large Geomagnetic Storm of April 17-18, 1965,"
    J. Geophys. Res., 72, 1813-1821 (1967a).

4. Gosling, J. T., et al., "Discontinuities in the Solar Wind Associated
    with Sudden Geomatric Impulses and Storm Commencements," J. Geophys.
    Res., 72, 2642-2650 (1969).

5. Ogilvie, K. W., L. F. Burlaga, and T. D. Wilkerson, "Plasma Observa-
    tions on Explorer 34," J. Geophys. Res., 73, 6809-6824 (1968).

6. Siscoe, G. L., "A Unified Treatment of Magnetospheric Dynamics with
    Applications to Magnetic Storms," Planet. Space Sci., 14, 947-967
    (1966).

7. Siscoe, G. L., V. Formisano, and A. J. Lazarus, "Relation Between
    Geomagnetic Sudden Impulses and Solar Wind Pressure Changes: An
    Experimental Investigation," J. Geophys. Res., 73, 4869-4874 (1986b).

8. Smith, E. J., et al., "Shocks and Storm Sudden Commencements," Solar
    Wind-Magnetosphere Coupling, edited by Y. Kamide and J. A. Slavin,
    pp. 345-365, Terra, Tokyo (1986).

9. Baumjohann, W. O., et al., "Magnetospheric Plasma Drifts During a
    Sudden Impulse," J. Geophys. Res., 88, 9287-9289 (1983).

10. Wilken, B., et al., "Magnetospheric Configuration and Energetic
    Particle Effects Associated with a SSC: Study of the CDAW 6 Event on
    March 22, 1979," J. Geophys. Res., 91, 1459-1473 (1986).

11. Voelker, H., "On Geomagnetic Pulsations Accompanying Storm Sudden
    Commencements and Sudden Impulses," Earth Planet. Sci. Lett., 1, 383
    (1966).

12. Saito, T., and S. Matushita, "Geomagnetic Pulsations Associated with
    Sudden Commencements and Sudden Impules," Planet. Space Sci., 15,
    573-587 (1967).

13. Kaufmann, R. L., and D. N. Walker, "Hydromagnetic Waves Exciteɑ During an SSC," J. Geophys. Res., 79, 5187-5195 (1974).

14. Fukunishi, H., "Latitude Dependence of Power Spectra of Magnetic Pulsations Near L = 4 Excited by SCCS and SIS," J. Geophys. Res., 84, 7191-7200 (1979).

15. Baumjohann, W. H., et al., "Resonant Alfven Waves Excited by a Sudden Impulse," J. Geophys. Res., 89, 2765-2769 (1984).

16. Friis-Christensen, et al., "Ionospheric Traveling Convection Vortices Observed Near the Polar Cleft: A Triggered Response to Sudden Changes in the Solar Wind," Geophys. Res. Lett., 15, 253-256 (1988).

17. Burlaga, L.F., "Micro-scale Structure in the Interplanetary Medium," Sol. Phys., 4, 67-92 (1968).

18. Burlaga, L. F., "Directional Discontinuities in the Interplanetary Magnetic Field," Sol. Phys., 7, 54-71 (1969).

19. Solodyna, C. V., J. W. Sari, and J. W. Belcher, "Plasma Field Characteristics of Directional Discontinuities in the Interplanetary Medium," J. Geophys. Res., 82, 10-14 (1977).

20. Ness, N. F., "Simultaneous Measurements of the Interplanetary Magnetic Field," J. Geophys. Res., 71, 3319-3324 (1966).

21. Burlaga, L. F., and N. F. Ness, "Tangential Discontinuities in the Solar Wind," Sol. Phys., 9, 467-477 (1969).

22. Siscoe, et al., "Power Spectra and Discontinuities of the Interplanetary Magnetic Field: Mariner 4," J. Geophys. Res., 73, 61-82 (1968a).

23. Nishida, A., and L. J. Cahill, Jr., "Sudden Impulses in the Magnetosphere Observed by Explorer 12," J. Geophys. Res., 69, 2243-2255 (1964).

24. Barcus, J. R., and T. J. Rosenberg, "Observations on the Spatial Structure of Pulsating Electron Precipitation Accompanying Low Frequency Hydromagnetic Disturbances in the Auroral Zone," J. Geophys. Res., 70, 1707-1716 (1965).

25. Oguti, T., et al., "Dayside Auroral Activity and Related Magnetic Impules in the Polar Cusp Region," J. Geomagn. Geoelec., 40, 387-408 (1988).

26. Song, P., R. C. Elphic, and C. T. Russell, "ISEE 1 and 2 Observations of the Oscillating Magnetopause," Geophys. Res. Lett., 15, 744-74 (1988).

27. Potemra, T. A., et al., "Multi-satellite and Surface Observations of Transient ULF Waves, in press, J. Geophys. Res. (1989).

28. Paschmann, G., et al., "Association of Low-Frequency Waves with Suprathermal Ions in the Upstream Solar Wind," Geophys. Res. Lett., 6, 209-212 (1979).

29. Fairfield, D. H., "Bow Shock Associated Waves Observed in the Far Upstream Interplanetary Medium," J. Geophys. Res., 74, 3541-3553 (1969).

30. Russell, C. T., et al., "Upstream Waves Simultaneously Observed by ISEE and UKS," J. Geophys. Res., 92, 7354-7362 (1987).

31. Spangler, S., et al., "An Observational Study of MHD Wave-Induced Density Fluctuations Upstream of the Earth's Bow Shock," J. Geophys. Res., 93, 845-857 (1988).

32. Plyasova-Bakounina, et al., "Pulsations in the Solar Wind and on the Ground," Planet. Space Sci., 26, 547-553 (1978).

33. Takahashi, K., R. L. McPherson, and T. Terasawa, "Dependence of the Spectrum of Pc3-4 Pulsations on the Interplanetary Magnetic Field," J. Geophys. Res., 89, 2770-2780 (1984).

34. Miletits, J. Cz., J. Vero, and W. F. Stuart, "Dynamic Spectra of Pulsation Events at L ~1.9 and L ~3.3," J. Atmos. Terr. Phys., 50, 649-656 (1988).

35. Lanzerotti, L. J., et al., "Polarization Characteristics of Hydromagnetic Waves at Low Geomagnetic Latitudes," J. Geophys. Res., 86, 5500-5506 (1981).

36. Yumoto, K., et al., "Propagation Mechanism of Daytime Pc3-4 Pulsations Observed at Synchronous Orbit and Multiple Ground-Based Stations," J. Geophys. Res., 90, 6439-6450 (1985).

37. Dungey, J. W., "Electrodynamics of the Outer Atmosphere," The Physics of the Ionosphere, pp. 229-236, 1954, Cambridge Conference, Physical Society, London (1955).

38. Atkinson, G., and T. Watanabe, "Surface Waves on the Magnetopsheric Boundary as Possible Origin of Long Period Geomagnetic Micropulsations," Earth Planet. Sci. Let., 1, 89-91 (1966).

39. Southwood, D. J., "The Hydromagnetic Stability of the Magnetospheric Boundary," <u>Planet. Space Sci.</u>, <u>16</u>, 587-605 (1968).

40. Southwood, D. J., "Magnetopause Kelvin-Helmholtz Instability, Magnetospheric Boundary Layers," edited by B. Battrick, <u>Eur. Space Agency Spec. Publ.</u>, ESA SP-148, 357-364 (1979).

41. Pu, Z.-U., and M. G. Kivelson, "Helvin-Helmholtz Instability at the Magnetopause: Soluation for Compressible Plasmas," <u>J. Geophys. Res.</u>, <u>88</u>, 841-852 (1983).

42. Mitchell, D. G., et al., "An Extended Study of the Low-Latitude Boundary Layer on the Dawn and Dusk Flanks of the Magnetosphere," <u>J. Geophys. Res.</u>, <u>92</u>, 7394-7404 (1987).

43. Kivelson, et al., "Global Compressional Oscillations of the Terrestial Magnetosphere: The Evidence and a Model," <u>J. Geophys. Res.</u>, <u>89</u>, 9851-9856 (1984).

44. Wolfe, A., L. J. Lanzerotti, and C. G. Maclennan, "Dependence of Hydromagnetic Energy Spectra on Solar Wind Velocity and Interplanetary Magnetic Field Direction," <u>J. Geophys. Res.</u>, <u>85</u>, 114-118 (1980).

45. Wolfe, A., et al., "ULF Geomagnetic Power at Cusp Latitudes in Response to Upstream Solar Wind Conditions," <u>J. Geophys. Res.</u>, <u>92</u>, 168-174 (1987).

46. Junginger, H., and W. Baumjohann, "Dayside Long-Period Magnetospheric Pulsations: Solar Wind Dependence," <u>J. Geophys. Res.</u>, <u>93</u>, 877-883 (1988).

47. McHenry, M. A., et al., "Observations of Ionospheric Convection Vortices: Signatures of Momentum Tansfer," <u>Multipoint Measurements of Magnetospheric Processes</u>, edited by C. T. Russell, IAGA, Espoo, Finland (1988).

48. Southwood, D. J., et al., "A Survey of Flux Transfer Events Recorded on the UKS Spacecraft Magnetometer," <u>Planet. Space Sci.</u>, <u>34</u>, 1349-1359 (1986).

49. Rijnbeek, R. P., et al., "A Survey of Dayside Flux Transfer Events Observed by ISEE 1 and 2 Magnetometers," <u>J. Geophys. Res.</u>, <u>89</u>, 786-800 (1984).

50. Russell, C. T., and R. C. Elphic, ISEE Observations of Flux Transfer Events at the Dayside Magnetopausae," <u>Geophys. Res. Lett.</u>, <u>6</u>, 33-36 (1979).

51. Gassmeier, K. H., et al., "Pc5 Pulsations and Their Possible Source Mechanisms: A Case Study," J. Geophys. Res., 55, 108-119 (1984).

52. Lanzerotti, L. J., and C. G. Maclennan, "Hydromagnetic Waves Associated with Possible Flux Transfer Events," Astrophys. Space Sci., 144, 279-290 (1988).

53. Farrugia, C. J., et al., "Flow in the Vicinity of Isolated Flux Tubed: Application to FTEs in the Incompressible Limit," Adv. Space Sci., 6, 129-134 (1986).

54. Farrugia, C. J., et al., "Field and Flow Perturbations Outside the Reconnected Field Line Region in Flux Transfer Events: Theory," Planet. Space Sci., 35, 227-240 (1987).

55. Paschmann, G., et al., "Plasma and Magnetic Field Characteristics of Magnetic Flux Transfer Events," J. Geophys. Res., 87, 2159-2168 (1982).

56. Lee, L. C., Y. Shi, and L. J. Lanzerotti, "A Mechanism for the Generation of Cusp-Region Hydromagnetic Waves," J. Geophys. Res., 93, 7578-7585 (1988).

57. Goertz, C. K., et al., "Observations of a Possible Ground Signature of Flux Transfer Events, J. Geophys. Res., 90, 4069-4078 (1985).

58. Lanzerotti, L. J., et al., "Possible Evidence of Flux Transfer Events in the Polar Ionosphere," Geophys. Res. Lett. 11, 1089-1092 (1986).

59. Lanzerotti, L. J., et al., "Ionosphere and Ground-Based Response to Field-Aligned Currents Near the Magnetospheric Cusp Region, J. Geophys. Res., 92, 7739-7743 (1987).

60. Gillis, E. J., et al., "Do Flux Transfer Events Cause Long-Period Micropulsations in the Dayside Magnetosphere?," J. Geophys. Res., 92, 5820-5826 (1987).

61. Lanzerotti, L. J., Comment on "Do Flux Transfer Events Cause Long-Period Micropulsations in the Dayside Magnetosphere?," by Fillis et al., J. Geophys. Res., 93, 2763-2764 (1988).

62. Gillis, E. J., et al., "Reply," J. Geophys. Res., 93, 2765-2766 (1988).

63. Hasegawa, A., "Drift Mirror Instabilities in the Magnetosphere," Phys. Fluids, 12, 2642-2650 (1969).

64. Southwood, D. J., "A General Approach to Low-Frequency Instabilities in the Ring Current Plasma," J. Geophys. Res., 81, 3340-3348 (1976).

65. Paschmann, G., et al., "The Plasma Instrument for AMPTE IRM, IEEE Trans. Geosci. Remote Sens., GE-23, 246-249 (1985).

66. Lueher, H., et al., "The IRM Fluxgate Magnetometer, IEEE Trans. Geosci. Remote Sens., GE-23, 259-261 (1985).

67. Russell, C. T., "The ISEE 1 and 1 Fluxgate Magnetometers, IEEE Trans. Geosci. Electron., GE-16, 239-242 (1978).

68. King, J. H., "Availability of IMP-7 and IMP-8 Data for the IMS Period," The IMS Source Book, edited by C. T. Russell and D. J. Southwood, pp.10-20, AGU, Washington, D.C. (1982).

69. Potemra, T. A., L. J. Zanetti, and M. H. Acuna, "The AMPTE CCE Magnetic Field Experiment," IEEE Trans. Geosci. Remote Sens., GE-23 , 246-249 (1985).

70. McEntire, R. W., et al., "The Medium-Energy Particle Analyzer (MEPA) on the AMPTE CCE Spacecraft," IEEE Trans. Geosci. Remote Sens., GE-23, 230-233 (1985).

71. Grubb, R. N., The SMS/GOES Space Environment Monitor Subsystem, NOAA Tech., Memo., ERL SEL-42 (1975).

72. Fennell, J. F., "Description of P78-2 (SCATHA) Satellite and Experiments, The IMS Source Book, edited by C. T. Russell and D. J. Southwood, pp. 65-81, AGU, Washingtion, D.C. (1982).

73. Gail, W. Γ , "Correlative Results from South Pole Station," 1981, Antartc. ﹍. U.S., 17, 225-228 (1982).

74. Lanzerotti, L. J., et al., "Magnetic Field and Particle Precipitation Observations at the South Pole, Antarct. J. U.S., 17, 235-236 (1982).

75. King, J. H., "Interplanetary Medium Data Book," NSSDC, Goddard Space Flight Center, Greenbelt, MD (1977).

76. Helliwell, R. A., "A Theory of Discrete Emissions from the Magnetosphere," J. Geophys. Res., 72, 4773-4790 (1967).

77. Walker, A. D. M., "Excitation of the Earth-Ionosphere Waveguide by Downgoing Whistlers, II, Propagation in the Magnetic Meridian," Proc. R. Soc. London, Ser. A., 340, 375-393 (1974).

78. Tsuruda, K., et al., "High Spatial Attenuation of the Siple Transmitter Signal and Natural VLF Chorus Observed at Ground-Based Chain Stations near Roberval, Quebec, J. Geophys. Res., 87, 742-750 (1982).

79. Helliwell, R. A., <u>Whistlers and Related Ionospheric Phenomena</u>, Stanford University Press, Stanford, CA (1965).

80. Heacock, R. R., and J. K. Chao, "Substorm-Associated Pulsations and Magnetopause-Magnetosheath Fluctuations," <u>J. Geophys. Res.</u>, <u>86</u>, 711-716 (1981).

81. Tsurutani, B. T., et al., "Drift Mirror Mode Waves in the Distant (X = 200 R$_E$) Magnetosheath," <u>Geophys. Res. Lett.</u>, <u>11</u>, 1102-1105, (1984).

82. Howe, H. C., and G. L. Siscoe, "Magnetopause Motions at Lunar Distance Determined from the Explorer 35 Plasma Experiment," <u>J. Geophys. Res.</u>, <u>77</u>m 6071-6086 (1972).

83. Anger, C. D., et al., "Long-Period Pulsations in Electron Precipitation Associated with Hydromagnetic Waves in the Auroral Zone," <u>J. Geophys. Res.</u>, <u>68</u>, 3306-3310 (1963).

84. Samsonov, S. N., et al., "The Relation Between Pulsations of Cosmic Radio Noise Levels and ELF-VLF Radiation, <u>Geomagn. Aeron., Engl. Transl.</u>, <u>27</u>, 556-560 (1987).

85. Walker, A. D., et al., "HF Radar Observations of Pulsations Near the Magnetospheric Cusp, <u>J. Geophys. Res.</u>, <u>91</u>, 8919-8928 (1986).

86. Perona, G. E., "Theory on the Precipitation of Magnetospheric Electrons at the Time of a Sudden Commencement," <u>J. Geophys. Res.</u>, <u>77</u>, 101-111 (1972).

87. Brown, R. R., "Sudden Commencement and Sudden Impulse Absorption Events at High Latitudes," <u>J. Geophys. Res.</u>, <u>78</u>, 5698-5702 (1973).

88. Brown, R. R., "Sudden Commencement Absorption Events at the Edge of the Polar Cap," <u>J. Geophys. Res.</u>, <u>82</u>, 2433-2435 (1977).

89. Gail, W. B. "Gurprespmamt Wave-Particle Interactions in a Dynamic Magnetosphere," Ph. D. Thesis, Dept. of Elec. Eng., Stanford Univ., Standford, CA (1987).

90. Gail, W. B., et al., "Characteristics of Wave-Particle Interactions During Sudden Commencements; 1, Ground-Based Observations," accepted by <u>J. Geophys. Res.</u>, (1988).

91. Chapman, S., and V. C. A. Ferraro, "A New Theory of Magnetic Storms, 1, The Initial Phase (Continued)," <u>Terr. Magn. Atmos. Elec.</u>, <u>36</u> 171-186 (1931).

92. Martyn, D. F., "The Theory of Magnetic Storms and Auroras," _Nature_, <u>167</u>, 92-94 (1951).

93. King, J. H., "Solar Wind Parameters and Magnetospheric Coupling Studies," in _Solar Wind-Magnetosphere Coupling_, edited by Y. Kamide and J. A. Slavin, pp. 163-177, Terra, Tokyo (1986).

94. Landau, L. P. and E. M. Lifshitz, _Fluid Mechanics_, pp. 457-459, Pergamon, New York (1959).

95. Paschmann, G., et al, "ISEE Plasma Observations Near the Subsolar Magnetopause," _Space Sci. Rev._, <u>22</u>, 717-737 (1978).

96. Olson, W. P., and K. A. Pfitzer, "Use of Geosynchronous Magnetometer Measurements to Estimate Solar Wind Parameters," _Eos Trans. AGU_, <u>68</u>, 1419 (1987).

97. Hess, W. N., _The Radiation Belt and Magnetosphere_, pp. 293-295, Blaisdell, Waltham, Mass. (1968).

98. Williams, D. J., "Magnetopause Characterisitics at 0840-1040 House Local Time," _J. Geophys. Res._, <u>85</u>, 3387-3395 (1980)

99. Roederer, J. G., "Dynamics of Geomagnetically Trapped Radiation," pp. 26-27, Springer-Verlag, New York (1970).

100. Sauer, H. H., and C. Rufenach, "Relationship of Geomagnetic Field at 6.6 R_E to Solar Wind Pressure," _Eos Trans. AGU_, <u>68</u>, 1418 (1987).

101. Konradi, A., "Rapid Increases in the Proton and Electron Fluxes in the Magnetosphere," _J. Geophys. Res._, <u>73</u>, 3449-3458 (1968).

102. Sibeck, D. G., et al., "Magnetic Field Drift Shell Splitting: Cause of Unusual Dayside Particle Pitch Angle Distributions During Storms and Substorms," _J. Geophys. Res._, <u>92</u> 13,485-13,497 (1987).

LABORATORY OPERATIONS

The Aerospace Corporation functions as an "architect-engineer" for national security projects, specializing in advanced military space systems. Providing research support, the corporation's Laboratory Operations conducts experimental and theoretical investigations that focus on the application of scientific and technical advances to such systems. Vital to the success of these investigations is the technical staff's wide-ranging expertise and its ability to stay current with new developments. This expertise is enhanced by a research program aimed at dealing with the many problems associated with rapidly evolving space systems. Contributing their capabilities to the research effort are these individual laboratories:

Aerophysics Laboratory: Launch vehicle and reentry fluid mechanics, heat transfer and flight dynamics; chemical and electric propulsion, propellant chemistry, chemical dynamics, environmental chemistry, trace detection; spacecraft structural mechanics, contamination, thermal and structural control; high temperature thermomechanics, gas kinetics and radiation; cw and pulsed chemical and excimer laser development, including chemical kinetics, spectroscopy, optical resonators, beam control, atmospheric propagation, laser effects and countermeasures.

Chemistry and Physics Laboratory: Atmospheric chemical reactions, atmospheric optics, light scattering, state-specific chemical reactions and radiative signatures of missile plumes, sensor out-of-field-of-view rejection, applied laser spectroscopy, laser chemistry, laser optoelectronics, solar cell physics, battery electrochemistry, space vacuum and radiation effects on materials, lubrication and surface phenomena, thermionic emission, photosensitive materials and detectors, atomic frequency standards, and environmental chemistry.

Electronics Research Laboratory: Microelectronics, solid-state device physics, compound semiconductors, radiation hardening; electro-optics, quantum electronics, solid-state lasers, optical propagation and communications; microwave semiconductor devices, microwave/millimeter wave measurements, diagnostics and radiometry, microwave/millimeter wave thermionic devices; atomic time and frequency standards; antennas, rf systems, electromagnetic propagation phenomena, space communication systems.

Materials Sciences Laboratory: Development of new materials: metals, alloys, ceramics, polymers and their composites, and new forms of carbon; nondestructive evaluation, component failure analysis and reliability; fracture mechanics and stress corrosion; analysis and evaluation of materials at cryogenic and elevated temperatures as well as in space and enemy-induced environments.

Space Sciences Laboratory: Magnetospheric, auroral and cosmic ray physics, wave-particle interactions, magnetospheric plasma waves; atmospheric and ionospheric physics, density and composition of the upper atmosphere, remote sensing using atmospheric radiation; solar physics, infrared astronomy, infrared signature analysis; effects of solar activity, magnetic storms and nuclear explosions on the earth's atmosphere, ionosphere and magnetosphere; effects of electromagnetic and particulate radiations on space systems; space instrumentation.